J Neurophysiol 96: 2613–2632, 2006.
First published July 19, 2006; doi:10.1152/jn.00188.2006.

Space–Time Separation During Obstacle-Avoidance Learning in Monkeys

Elizabeth Torres and Richard Andersen
Biology Division, California Institute of Technology, Pasadena, California

Submitted 20 February 2006; accepted in final form 16 July 2006

Torres, Elizabeth and Richard Andersen. Space–time separation during obstacle-avoidance learning in monkeys. *J Neurophysiol* 96: 2613–2632, 2006. First published July 19, 2006; doi:10.1152/jn.00188.2006. Is the movement duration time known before we move? To answer this question, a new experimental paradigm is introduced that for the first time monitors the acquisition of a new motor skill in rhesus monkeys. Straight reaches were interleaved with reaches around physical obstacles that elicited a different path geometry. Curved and longer spatial paths were immediately resolved and consistent over months of training. A new temporal strategy separately evolved over repetitions from multiple to a single velocity peak. We propose that the obstacle-avoidance spatial paths were resolved before motion execution and used as reference in the computation of the new dynamics. Path conservation from the first trial occurred both at the hand and at the joint angle levels, whereas the speed profile dramatically changed over time. The spatial solution required no learning and was anticipated by the spontaneous repositioning of the initial arm posture. The learning was in the temporal domain, involving the adjustment of the speed during the motion's first impulse. Within the movement initiation, the partial distance traveled by the hand up to the first velocity peak was finely tuned under a constant time. For a given space location, the time of the first impulse remained robust to learning, but significantly shifted for different targets and obstacle configurations. Differences in the temporal-related parameters across time provided a clear distinction between learning and automatic behavior.

INTRODUCTION

Right before competing at the Olympics, gymnasts are so proficient at performing their routine that if they rehearse it 10 times, 10 times it will yield almost the exact same duration and invariably the same speed profile (McNitt-Gray 2000). Across repetitions, for each point in their motion path there will be a coincidence in space and time. Likewise, when subjects perform reaching movements in a motor control experiment, their timing achieves very precise duration and a consistent temporal strategy. But what happens during the course of learning a new motion? Is the system aware of how long every new movement should take? Is there a predefined speed profile? And if so, where does this ideal timing come from?

For years, the field of motor control has focused on reaching movements that are highly automatic. They consistently follow a spatiotemporal profile that for the nonredundant cases can be derived by solving the equations of motion under the classical mechanics scheme. The movement trajectories minimize the energy expressed as an integral over a predefined time interval. The energy-minimizing solution simultaneously describes a motion in space and time (Alexander 1997; Flash and Hogan 1985; Harris and Wolpert 1998; Todorov and Jordan 2002; Uno et al. 1989, 1995). Therefore space and time are tightly coupled. Current computational models of motor control follow this approach when solving the motion dynamics (see reviews by Jordan and Wolpert 1999; Todorov 2004) and often argue over whether the kinematics (position, velocity, etc.) or the dynamics (forces and force-related quantities) are more important for the planning of a motion. Regardless of the side one takes in this argument, the temporal aspects of the movement have already been predefined, so they do not form part of the learning process.

The developmental literature, however, teaches us that infants master reaching and grasping motions at an early age and that the process can be clearly divided into two phases: 4 to 8 wk after reach onset (occurring at 20 wk) there is rapid improvement of motion parameters in hand and joint space, followed by a second phase of fine-tuning where more gradual changes (such as a reduction in path variability) are observed that last well into the 2 yr of age (Konczak and Dichgans 1997). Thus these studies already hint at some separable process during early learning.

We also know from studies involving adult humans that subjects can traverse the same planar reaching hand path with different speeds (and loads) (Atkeson and Hollerbach 1985), the same postural (and three-dimensional hand) paths under different speeds during reaching (Nishikawa et al. 1999), and orientation matching (Torres and Zipser 2004). However, why or how this should be possible has not been formally addressed with a computational theory.

This study explores the question of space–time decoupling during learning. To elicit the need for learning, and to monitor learning over time, we introduce a novel experimental paradigm that during each session forces the system to switch between two tasks. The paradigm interleaves straight-line reaches with novel reaches around obstacles that significantly change the curvature and length of the hand paths, thus demanding movements of longer duration (see METHODS and Fig. 1*A* for further details). The key element in this paradigm is that the new task is simple enough that it requires no training of the animals, yet complex enough that it changes the arm path geometry and calls for the learning of a new spatiotemporal strategy.

Two rhesus monkeys were the subjects in this experiment as the study of the neurophysiological aspects of this problem is currently under way. No explicit instructions could be given to the subjects on how to execute the task, so the acquisition of the new motor skill occurred naturally. Both animals were initially naïve to the obstacle task. Their performance revealed

Address for reprint requests and other correspondence: E. B. Torres, Biology Division, California Institute of Technology, 333 Beckman Labs, Biology M/C 216-76, Pasadena, CA 91125 (E-mail: etorres@vis.caltech.edu).

The costs of publication of this article were defrayed in part by the payment of page charges. The article must therefore be hereby marked "*advertisement*" in accordance with 18 U.S.C. Section 1734 solely to indicate this fact.

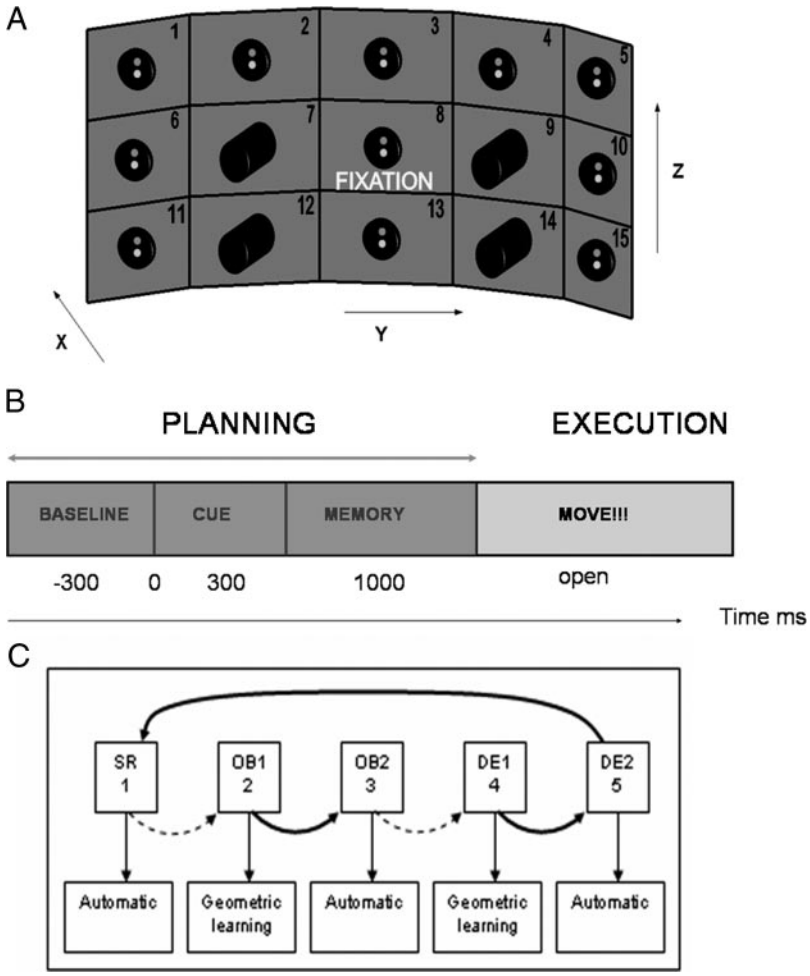

FIG. 1. *A*: schematic of the experimental board shows the 6 most affected targets (on locations 1, 5, 6, 10, 11, and 15), the 4 obstacle locations used in the experiment, and the fixation button. *B*: temporal structure of one trial in the delayed reaching task is divided into the premovement time and the execution time. Planning involves fixating straight ahead while holding the button at a given initial posture for 300 ms (proprioceptive input about initial posture), a target flashes in the periphery (visual input, cued for 300 ms) and the animal must maintain fixation, then hold the action plan during the memory period (transform goals into impending action). Movement initiates after the fixation light goes off indicating the end of the delay. This delay randomly changes between 800 and 1,000 ms. No lower bound on movement duration is imposed, but if the animal does not reach after 3 s, the trial is aborted. *C*: 5 behavioral epochs defined for analysis: *1*) First block of simple straight reaches (SRs) automatic with very stereotypical tempo: consistent time duration and speed profile. Well-coordinated arm motions, highly synchronized in space and time. *2*) First 10 trials of obstacle-avoidance reaches (early OB-learning), geometric-based learning, time estimated from distance. Former temporal strategy proved obsolete under new geometry. Spatial strategy solved before movement. *3*) Last 10 trials of obstacle-avoidance reaches (late OB-automatic) automatic period. Spatial consistency with repeatability of temporal parameters: similar duration and unimodal speed profiles. Arm motions coupled in space and time. *4*) First 5 trials of deadaptation (DE), (early DE-learning) geometric-induced learning. OB-spatiotemporal residual effects. *5*) Last 5 trials of deadaptation (late DE-automatic). All features of straight reaches recovered.

that during the learning period, the system neither had knowledge of how long the movement would take, nor did it show a proficient temporal strategy to traverse the new spatial path that did satisfy the task goals. The data suggest that the path geometry was promptly resolved and conserved while the optimal timing was being learned. This decoupling was observed not only during the experimental session of one day but also across many consecutive days. In this sense, the acquisition of consistency in the temporal profile of the new motion signaled automaticity.

METHODS

Two male rhesus macaques were trained to perform delayed center-out reaches (SRs) in the dark with the left arm to six to 14 targets located on a vertically oriented push-button board (Fig. 1*A*). The animals sat in a primate chair with their heads fixed 24 cm away from the board. The buttons were 3.7 cm in diameter and set 7.5 cm apart. Each button had red and green light-emitting diodes (LEDs) set behind a translucent window. The red LED instructed eye fixation and the green LED instructed initial hand position. All trials started with the illumination of the red and green LEDs at the fixation button, located directly in front of the animal at eye level. A target button located at the periphery turned on the green light to cue (for 300 ms) the reach location in a pseudorandom order. After a variable delay period of 700–1,000 ms the straight-ahead fixation red and green LEDs turned off, instructing the animals to reach to the peripheral location. Then a small amount of juice rewarded the animals. Blocks of straight reaches were alternated with blocks of reaches around cylindrical obstacles (6 cm in length, 3.7 cm in diameter). Two or four buttons were blocked by obstacles on one or both sides of the board, respectively. The data reported here correspond to blockage of two buttons on one or both sides, positioned ipsi- and/or contralateral to the moving arm on the way to the targets (Fig. 1*A*). Both animals were naïve to the obstacle task, so that learning could be monitored both on a daily basis (locally) and across weeks of training (globally) until the movement reached a ballistic feature as measured by the stereotypical newly acquired speed profiles in the obstacle task and by the absence of "residual" deadaptation paths in the early trials after obstacle removal. During the obstacle condition, the animals did not have visual feedback of the physical obstacles. The arm was not constrained in any way. The hand moved in three dimensions.

The experimental paradigm consisted of a first block of straight reaches (10–15 trials), a second block of 30 trials of reaches around obstacles, and a third block of 30 trials of straight reaches after obstacle exposure. The animals saw the experimenter both positioning and removing the obstacles with the lights temporarily on. An electromagnetic tracking system (Polhemus Fastrak) recorded the arm motions in space at a sampling rate of 120 Hz for four sensors. Three sensors were mounted on small pieces of Plexiglas and attached with thick Velcro to the left sleeve of a rhesus primate jacket (Harvard Apparatus). The fourth sensor was used separately to measure shoulder position. In figures in the main text, filled cylinders mean that there was an obstacle at that location during that block of trials, whereas wire-frame cylinders mean that there was no obstacle present in that block. The wire-frame cylinder represents the locations where the obstacle was.

Obstacle properties and configurations affect reaches differently

Several obstacle shapes and lengths were explored before settling on the chosen one. One obstacle alone on location 7 or/and 9 did not elicit sufficiently curved paths to cause temporal adaptation. It should be noted that only when two obstacles were positioned at locations 7, 12, or/and 9, 14, did we observe highly curved arm paths that resulted in temporal adaptation, causing aftereffect paths; otherwise, most movements showed from the first trial a single bell-shaped temporal strategy similar to that from the straight reaches. The changes were in the magnitude of the speed (Fig. 2*A*). This is important to keep in mind to replicate our results. There will be temporal adaptation only if the geometric deformation of the paths is significant enough to call for a change in the temporal strategy previously used for straight reaches. In addition, the length and shape of the obstacles will affect the path-solution strategy (Fig. 2*B*).

Data analysis

We distinguished the geometric-based temporal learning from the automatic epochs based on the speed profiles [i.e., learning (slow broken profiles) vs. automatic (fast smooth profiles)] and for data analysis we partitioned the blocks into the first 10 trials (early) versus the last 10 trials (late) in the order in which they were acquired. To extract the motion from the sensors' output, we defined the beginning and the end of the movement as 5% maximum velocity along a speed profile. For each trajectory, we determined the points where the velocity dropped to 5% of the maximum and eliminated the data beyond those points. Overall movement speed ranged from 70 to 185 cm/s (minimum and maximum, respectively).

A measure of curvature K was determined by projecting each point of the curved path onto the straight line joining the initial and final points and obtaining the normal distance from each point along the curved path to its corresponding projection on the straight line (range 10–26 cm). A perfectly straight path would have $K = 0$.

The Wilks's test statistic (Rencher 1995) for points of the hand paths was used in standard multivariate ANOVA on the positional hand paths of Fig. 4, *A* and *B* and in the analysis of the postural paths (Table 1).

RESULTS

The placement of an obstacle on the way to the visual targets demanded changes in the spatial route of the hand, thus influencing the entire arm path. To evoke the space–time decoupling and to bring a strong motor learning component to the task, it was necessary to take into consideration the obstacle's location, size, and shape. The results discussed here are specific to a context that sufficiently altered the motion geometry and therefore induced the space–time separability. In contexts that evoke simpler motions this decoupling will go unnoticed.

Cognitive goals determine the spatial path before movement initiation

HAND SPACE. During the obstacle condition both subjects resolved the spatial solution paths with no errors, i.e., without colliding against the obstacles or missing the targets. The spatial solution paths complied with distance-based constraints arising from the obstacle location, shape, size, and the fixed distances between the primate chair and the board. These visually determined task constraints influenced the choice of path to prevent not only the hand but also the rest of the arm from colliding with the obstacles in complete darkness. A geometric model of obstacle-avoidance path specification based on these kinds of goals and constraints for an arm with degrees of freedom (df) = 7 inspired the design of this experiment (see APPENDIX). However, we reserve for the discussion some key aspects of this theoretical approach. Figure 2*A* versus Fig. 3 contrasts the differences in solution paths resulting from obstacle positioning. On average, most paths in Fig. 2*A* inherited the same temporal strategy as those in the straight reaches. Temporal learning was far less evident than that observed when two obstacles were present, as in Fig. 3. In this case paths were much longer and curved, rendering the former speed profiles obsolete for the new geometry [consistent with earlier findings by Abend et al. (1982)]. Figure 2*B* shows the choice of spatial route as a function of obstacle size. For a longer cylinder movement to all three targets avoided the obstacle by passing below it. For a shorter cylinder movements to one of the targets avoided the obstacle by passing above it.

The chosen spatial paths were successful from the first trial and remained consistent over the course of many trials. This is shown in Figs. 3 and 4. Figure 3 illustrates the path similarity during the obstacle block. Figure 4*A*, *right* shows the overlapping three-dimensional (3D) confidence regions around the mean paths for the obstacle condition. The obstacle-avoidance 3D spatial paths of the hand were not separable according to Wilks's test statistic (Table 1) (Rencher 1995).

POSTURE SPACE. Across targets this consistency in the hand paths extended to the forearm and to the upper arm. It was also reflected in the seven-dimensional joint angle positional paths that best reconstructed the motion sensor paths [reconstruction method described in detail in Torres (2001)]. Figure 5*A* shows the seven-joint-angle paths resampled in space (100 points, with no temporal information), where no significant differences were found for all joint angles according to Wilks's lambda ratio (Table 1) between the learning and the automatic epochs across all targets. Notice, however, that for paths to the most affected ipsilateral target shown in this figure, the individual hand abduction joint angle showed differences between the first few trials in the early obstacle-avoidance epoch compared with the last trials of the late epoch. This revealed that the major transport components of the reach involving flexors and extensors remained consistent as the tempo was being learned. Figure 5*B* illustrates the similarity of the paths for the learning and the automatic phases for each one of the sensors at the hand, the forearm, and the upper arm. These results for one subject were the same for the second subject.

In anticipation of the obstacle-avoidance solution path both animals spontaneously repositioned the initial posture (Fig. 5*C*, Table 1). Accordingly, the final posture at the target was also statistically different when comparing the straight versus obstacle-avoidance postural paths (Fig. 5*D*, Table 1).

Geometric-based (temporal) learning: when movement timing is not predefined

The transition from simple straight reaches (SRs) to early obstacle avoidance (OB-learning) demanded drastic changes in the geometry of the movement. These large geometric changes influenced the motion dynamics, thus changing the temporal course along the spatial path. Table 1 (*columns 1* and *2*) shows

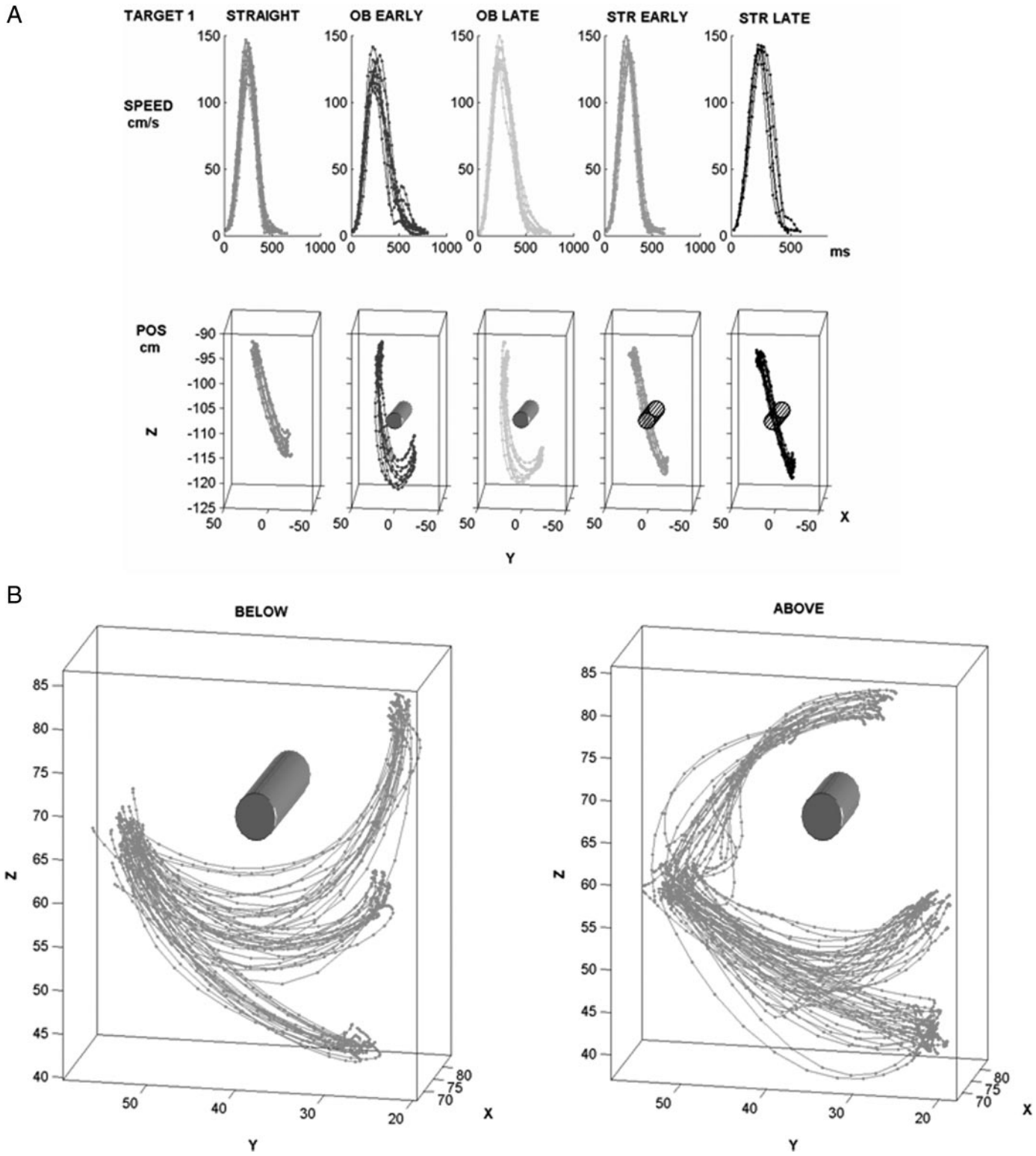

FIG. 2. Obstacle positioning and size affected the spatiotemporal strategy. *A*: one obstacle positioned on locations 7 or/and 9 on the board sketched in Fig. 1 did not significantly change the time course of the motion. Task switching was immediate. *B*: size of the obstacle affected the spatial strategy for motions to the same board location 9. For the longer obstacle, the hand paths passed below it. For the shorter obstacle, some hand paths passed above it.

that across targets that are maximally affected by the obstacle there were significant differences in path length, curvature, movement duration, and number of velocity peaks compared with those of straight reaches.

The required changes in spatial path and movement timing followed a clear order. Although the spatial solution path for obstacle avoidance was anticipated at the postural level, succeeded from trial one and was conserved for the

TABLE 1. *Analysis of postural paths*

	Ipsilateral Targets														
	Board Location 1					Board Location 6					Board Location 11				
	1–2	2–3	3–4	4–5	5–1	1–2	2–3	3–4	4–5	5–1	1–2	2–3	3–4	4–5	5–1
Time	1	1	1	1	0	1	1	0	0	0	1	0	0	1	0
(*P* value)	(0)	(0.04)	(0.003)	(0.009)	(0.59)	(0)	(0.008)	(0.19)	(0.17)	(0.36)	(0.009)	(0.9)	(0.16)	(0.04)	(0.22)
# Vel Peaks	1	1	0	0	0	1	1	0	0	0	0	0	0	0	0
(*P* value)	(0.004)	(0.017)	(0.556)	(0.330)	(0.55)	(0.017)	(0.006)	(0.673)	(0.660)	(0.129)	(0.628)	(0.448)	(0.232)	(0.336)	(0.14)
Path length	1	0	1	1	1	1	0	1	0	0	1	0	1	1	0
(*P* value)	(0)	(0.6)	(0.002)	(0.04)	(0.02)	(0)	(0.5)	(0.01)	(0.8)	(0.15)	(0)	(0.6)	(0.03)	(0.01)	(0.2)
K	1	0	1	1	0	1	0	1	0	1	1	0	0	0	0
(*P* value)	(0)	(0.20)	(0.002)	(0.015)	(0.428)	(0.0)	(0.10)	(0.003)	(0.56)	(0.023)	(0.29)	(0.47)	(0.644)	(0.38)	(0.88)
7 JA Path	0.0035	0.3852	0.0332	0.1252	0.1839	0.0048	0.2368	0.0260	0.0342	0.1956	0.0173	0.2162	0.0724	0.0591	0.1773
(λ) mean SD	0.003	0.172	0.024	0.054	0.094	0.004	0.155	0.024	0.023	0.092	0.009	0.009	0.066	0.102	0.021
Init JA (λ) value	0.0071	0.2680	0.0646	0.0506	0.1874	0.0152	0.1785	0.1130	0.0812	0.1981	0.0138	0.1997	0.1332	0.1049	0.2014
End JA (λ) value	0.0062	0.2461	0.0260	0.0889	0.1763	0.0210	0.4184	0.0804	0.0962	0.2105	0.0103	0.5770	0.0296	0.1357	0.1884
Hand path	0.0205	0.6087	0.2611	0.2077	0.3178	0.0498	0.6771	0.0996	0.1499	0.2981	0.0498	0.6771	0.0996	0.0981	0.4499
(λ) mean SD	0.032	0.269	0.062	0.012	0.060	0.036	0.185	0.064	0.148	0.059	0.036	0.185	0.064	0.059	0.149
	Contralateral Targets														
	Board Location 5					Board Location 10					Board Location 15				
Time	1	0	1	1	0	1	0	1	0	0	1	0	1	0	1
(*P* value)	(0)	(0.3)	(0.007)	(0.004)	(0.36)	(0)	(1)	(0.022)	(0.58)	(0.79)	(0.001)	(0.13)	(0.008)	(0.25)	(0.030)
# Vel Peaks	1	0	1	1	0	0	0	0	0	0	0	0	0	0	0
(*P* value)	(0.005)	(0.26)	(0.038)	(0.024)	(0.14)	(0.33)	(0.36)	(0.47)	(0.55)	(0.49)	(0.33)	(0.28)	(0.19)	(1)	(0.77)
Path length	1	0	1	1	1	1	0	1	0	1	1	0	1	1	0
(*P* value)	(0)	(0.5)	(0.004)	(0.01)	(0.02)	(0)	(0.8)	(0.02)	(0.7)	(0.03)	(0)	(0.6)	(0.05)	(0.02)	(0.6)
K	1	0	0	1	0	1	0	1	1	1	1	0	0	0	0
(*P* value)	(0.02)	(0.26)	(0.61)	(0.067)	(0.96)	(0.04)	(0.39)	(0.006)	(0.007)	(0.018)	(0)	(0.70)	(0.15)	(0.52)	(0.59)
7 JA Path	0.0057	0.1833	0.1735	0.1010	0.1911	0.0045	0.2160	0.0780	0.0299	0.2411	0.0131	0.3380	0.0894	0.1321	0.2208
(λ) mean SD	0.004	0.005	0.013	0.014	0.019	0.005	0.075	0.050	0.038	0.029	0.009	0.155	0.072	0.093	0.010
Init JA (λ) value	0.0096	0.1907	0.1323	0.0419	0.1796	0.0107	0.2432	0.0552	0.0096	0.2183	0.0145	0.2869	0.1056	0.1264	0.2166
End JA (λ) value	0.0069	0.1904	0.1695	0.0786	0.1944	0.0057	0.1792	0.1266	0.0302	0.2134	0.0158	0.2307	0.1642	0.1704	0.2300
Hand path	0.0208	0.5517	0.1012	0.0590	0.4222	0.0167	0.7290	0.2034	0.2155	0.3225	0.0222	0.6438	0.2096	0.0345	0.3542
(λ) means SD	0.019	0.135	0.072	0.042	0.146	0.013	0.125	0.059	0.178	0.015	0.008	0.134	0.128	0.015	0.214

Columns represent comparison between two behavioral epochs: (1–2) refers to SR–OB-learning; (2–3) is OB-learning–OB-automatic; (3–4) is OB-automatic–DE-learning; (4–5) is DE-learning–DE-automatic; (5–1) is DE-automatic–SR. Parameters of interest are: movement duration time in milliseconds, number of velocity peaks per trial, the path length in centimeters, the measure of curvature K in centimeters (distance from each point along the curve to its projection onto the straight line), the seven joint angles of the arm in degrees, including the full path and the final posture, and the hand positional path in centimeters. Entry values are from the one-tailed critical t-test for two groups at the 0.01 alpha-level. Each entry has the H = 1/0 value for the Matlab convention, with H = 0 meaning "Do not reject null hypothesis at significant level of alpha." The P value is shown in parentheses. Early and late OB and DE include the first and last five trials of the block, respectively. Shaded boxes signify "Do not reject null hypothesis for group means equality." Time duration (in milliseconds) was obtained from the number of points in the motion path at a sampling rate of 40 Hz. It ranged between 420 and 1,300 ms for ipsilateral targets and between 500 and 1,000 ms for contralateral targets. Path length ranged between 37 and 79 cm for ipsilateral targets and between 39 and 105 cm for contralateral targets. Deviation from the straight line ranged between 14 and 26 cm for ipsilateral targets and between 21 and 27 cm for contralateral targets. Postural analysis for seven joint angles of the arm was carried out using Wilks's lambda. Reject null hypothesis if $\Lambda \leq \Lambda_{\alpha,p,v_H,v_E}$, where $\alpha = 0.05$, $p = 7$, and $v_H = k - 1$, $v_E = k(n - 1)$ are the degrees of freedom for hypothesis and error terms, respectively, for the joint-angles case. The number of samples $k = 2$ and the number of points per sample $n = 5$, taking the first five trials in OB and DE early and the last five trials in OB and DE late. $\Lambda_{\alpha = 0.05,p = 7,v_H = 1,v_E = 8} = 0.176$ taken from Rencher (1995). Joint angle and hand paths were resampled to have 100 points. Lambda values are obtained for each point in the path. Entries are the mean lambda value over the 100 points and the SD. The individual lambda values for the initial and final postures are also shown. Critical value for the hand path is for $\alpha = 0.05$, $p = 3$, and $\Lambda_{\alpha = 0.05,p = 3,v_H = 1,v_E = 8} = 0.295$.

remaining trials, the temporal path that accommodated it had to be learned. This was evidenced in the changes observed in the time duration, the number of velocity peaks, and the evolution of the first significant velocity peak value from low to high from OB-learning to OB-automatic (one-tail critical t-test for two groups at the 0.01 alpha-level; Tables 1 and 2). Figure 4*B* contrasts the jerky versus the smooth speed profiles during the learning and the automatic phases of motion.

A temporal point may help to construct the new efficient timing

Recent work proposed the existence of a spatial via point to aid in sequentially forming complex curved motions (Hatsopoulos et al. 2003; Morasso and Mussa-Ivaldi 1982; Viviani and Flash 1995; Viviani and Schneider 1991; Wada and Kawato 2004). Although the thought of breaking up the spatial paths according to some geometric prescription and storing

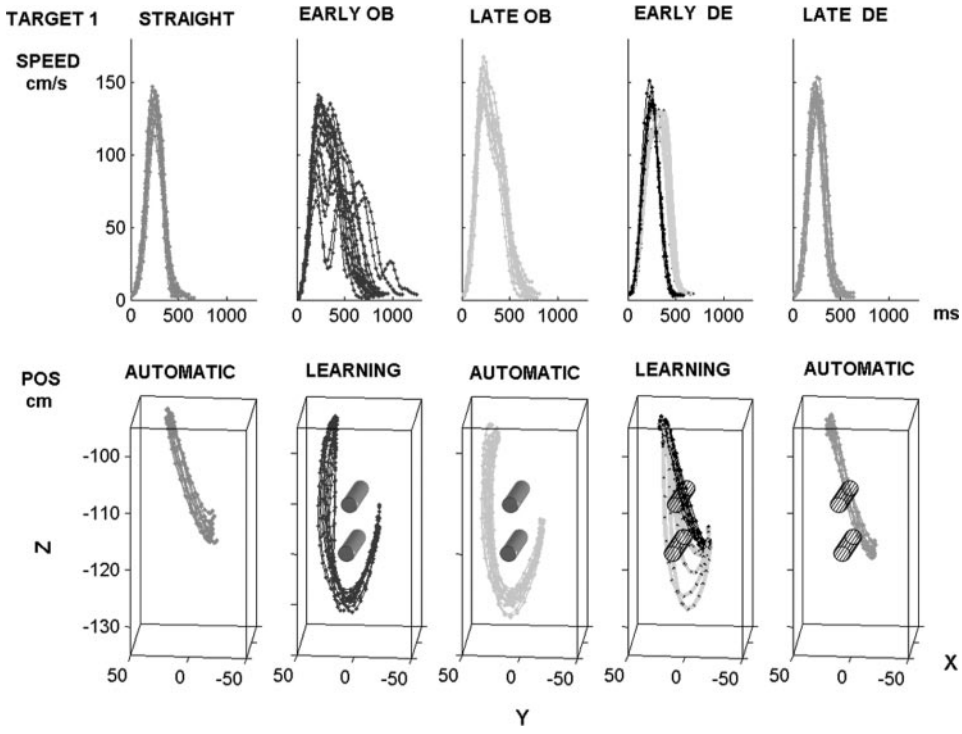

FIG. 3. Spatial and temporal path evolution for the target on board location 1 (ipsilateral) across the 5 behavioral epochs defined in Fig. 1*B*. Highly variable temporal course across trials during the OB block (movement duration ranged from 1,250 to 700 ms). Peak velocity value increased monotonically to a stable value from OB-learning to OB-automatic. Early DE-learning speed profiles (4–5 first trials) changed from bimodal to a single peak. Curved "residual" paths converged to straight-reaches paths.

these spatial segments as "motor primitives" is intuitively sound, our results suggest an additional and new idea: to use temporal rather than spatial points as reference in the search for a smooth motion and to store temporal rather than spatial information as motor primitives. This temporal point should be tied to the tangential peak velocity of the movement in relation to the goals of the task, not to an arbitrary point along the spatial path. Tangential peak velocity points are relevant because they relate to curvature and deceleration phases of the motion. Peak velocity and thus first deceleration were consistently reached near to the point of highest curvature along the path, regardless of whether the system was still in the learning or in the automatic phase. In other words, the first impulse of the motion strongly determined how the system temporally moved along the remainder of the path.

Figure 6, *A* and *B* shows this for both the learning and the automatic phase and aid in examining the validity of this new idea of forming motor primitives in the temporal domain. The figure contrasts the differences in the point along the spatial path where the first velocity peak was reached during the learning and the automatic phases. The 10 first and 10 last trials in the block where used in the analysis. Initially there was a region of interest in space, plotted here for each trial (Fig. 6*A*). This region eventually converged to a tight cluster, a single location in space (Fig. 6*B*). Each point is plotted at the end of the distance traveled before the hand started to slow down.

Parenthetically, if this motion had been studied only after it was learned (in its automatic phase), this location would have been designated as the spatial via point. The interesting aspect of this temporal search process is that all of these points, those in the spread-out region and those in the tight cluster, hit the peak velocity between 200 and 250 ms with no significant differences between the learning and the automatic phases. The ANOVA (Fig. 6*C*) revealed no separation between the means of the two groups; early-slow versus late-fast [$F = 0 < (F^*_{0.05,1,18} = 4.41, F^*_{0.01,1,18} = 8.29)$, $P = 1$], but significant differences when compared with the straight reaches [$F = 8.47 > (F^*_{0.05,2,27} = 3.35, F^*_{0.01,1,18} = 5.48)$, $P = 0.001$]. Within the obstacle-avoidance block what significantly changed was the value of the peak velocity (one-tail critical *t*-test for two groups at the 0.01 alpha-level; Table 2). Initially this value was comparable to or even lower than that in straight reaches but it became significantly higher in the automatic phase, where it reached a plateau reflected in the acquired consistency of the space location where it settled.

Because during obstacle avoidance the total path length of the motion remained stable and the time to reach the first peak was reliable, as the distance traveled up to that point in time changed, so did the peak velocity value. Figure 6*D* shows significant separation of the means for the distance traveled along the path up to the temporal point when comparing the early and late epochs of the OB block [$F = 16.15 > (F^*_{0.05,1,18} = 4.41, F^*_{0.01,1,18} = 8.29)$, $P = 0.0008$]. Comparison of straight reaches to the early and late OB epochs revealed significant differences as well [$F = 12.06 > (F^*_{0.05,2,27} = 3.35, F^*_{0.01,2,27} = 5.48)$, $P = 0.0002$]. Figure 6*E* shows significant differences for the peak velocity values when comparing straight to early and late OB-avoidance reaches ($F = 16.15$, $P = 0$).

The trend observed in Fig. 6, *D* and *E* shows a cautious strategy for the peak velocity of the motion where the system initially moved significantly slower than it could afford, increasing the velocity as it covered more distance in the same amount of time. It is possible that an overall higher-level plan similar to that in straight reaches is evidenced in these data, that is, to reach the peak velocity value at midway along the spatial path. However, the hand trajectories in Fig. 6*B* suggest that dynamics constraints for the highly curved motion settled this point at one third of the total path length.

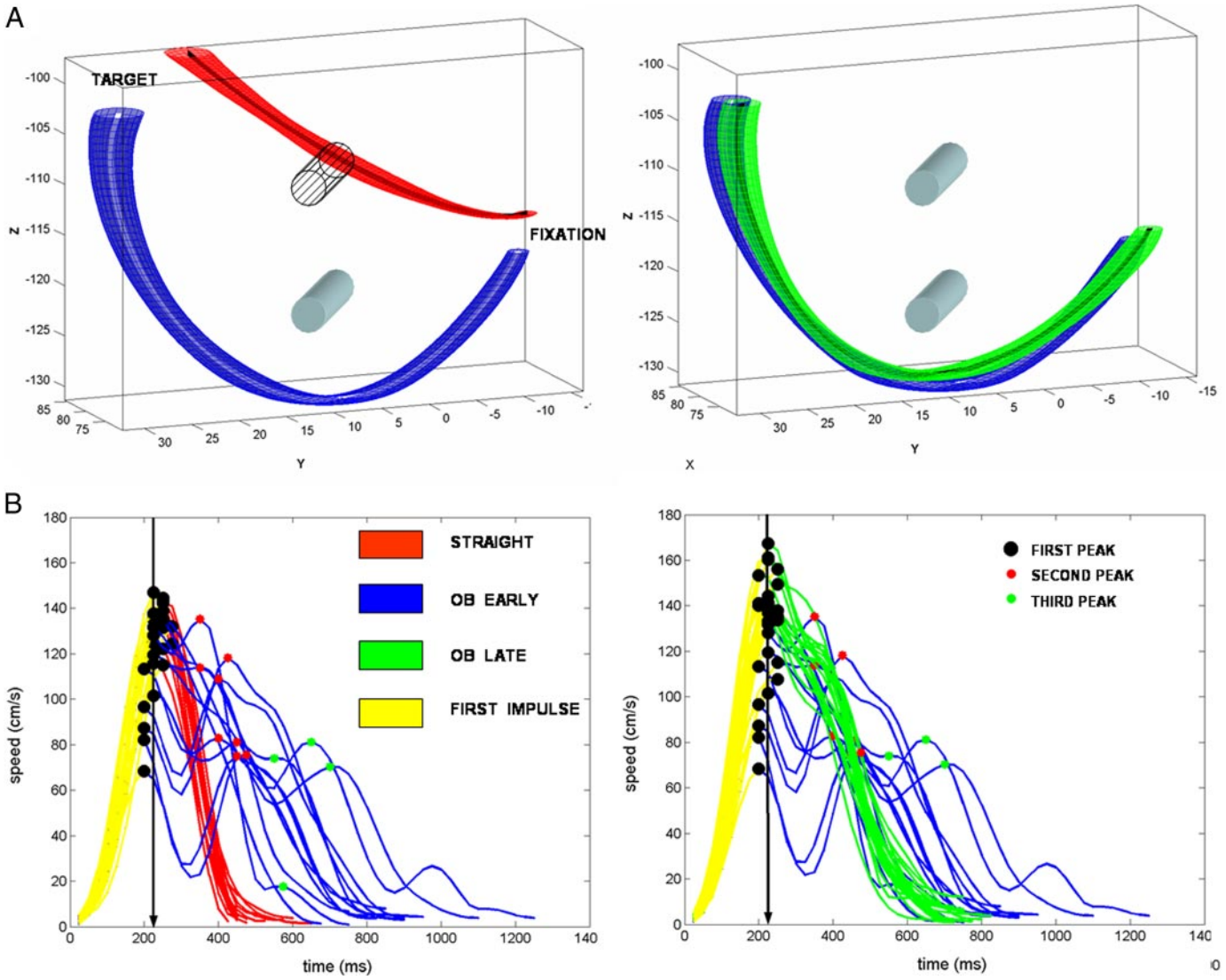

FIG. 4. Three-dimensional (3D) statistical analyses of hand sensor output for positional paths. *A*: comparison between straight reaches and OB-learning vs. OB-learning and OB-automatic. Straight reaches paths differed significantly from OB-learning, but OB-learning vs. OB-automatic were consistent with overlapping means and confidence 3D regions. *B*: effect of the OB on the speed profiles. Similar spatial paths in OB-avoidance had different peak velocity values and multiple velocity peaks. Both parameters converged. Arrow marks the time to reach the first velocity peak, which was the same across all OB-avoidance trials. For each path in each trial the black dot marks the 1st peak, the red asterisk the 2nd peak, and the green asterisk the 3rd peak. Yellow portion marks the first impulse of the motion.

A longitudinal analysis for board locations 1 and 5 on the evolution of the time to reach the first peak, the total path length and the value of the first velocity peak over 15 consecutive days of experiments revealed consistency in the first two parameters and significant changes on the third. During each experimental session the time to first peak and the path length were the same during both the learning and the automatic OB-avoidance phases with a separation between ipsi- and contralateral space locations. In contrast, the value of the first velocity peak showed significant changes from slow OB-learning to fast OB-automatic during each experimental session and across time. Figure 7, *A* and *B* shows that both the time to reach the first peak and the path length were more robust to learning, with a slight (nonsignificant) trend for path length to decrease when comparing day 1 to day 15. Figure 7*C* shows that the value of the first velocity peak changed each day and evolved over time. The first day there was a significant separation of the means. The overlap starts at the fifth consecutive day of training. The error bars represent unit SDs. The *inset* in Fig. 7*E* shows the evolution across trials for each one of the days. Notice that on day 15 the value of the peak velocity overlapped for the earlier and later trials. There was also an overall increase in this parameter when compared with days 5 and 10. Figure 7*D* shows (for the most affected ipsilateral target on board location 1) the effect of learning on the distance traveled up to the time when the motion reached the first velocity peak. Initially these values were significantly different between the early and the late OB-avoidance epochs, but as time progressed their mean values became closer. A similar result was observed for the contralateral case.

The reliability of the time to first peak across days of learning for the board locations that were most affected by the obstacle poses the question of whether this point in time arises independent of the obstacle configurations, or the target loca-

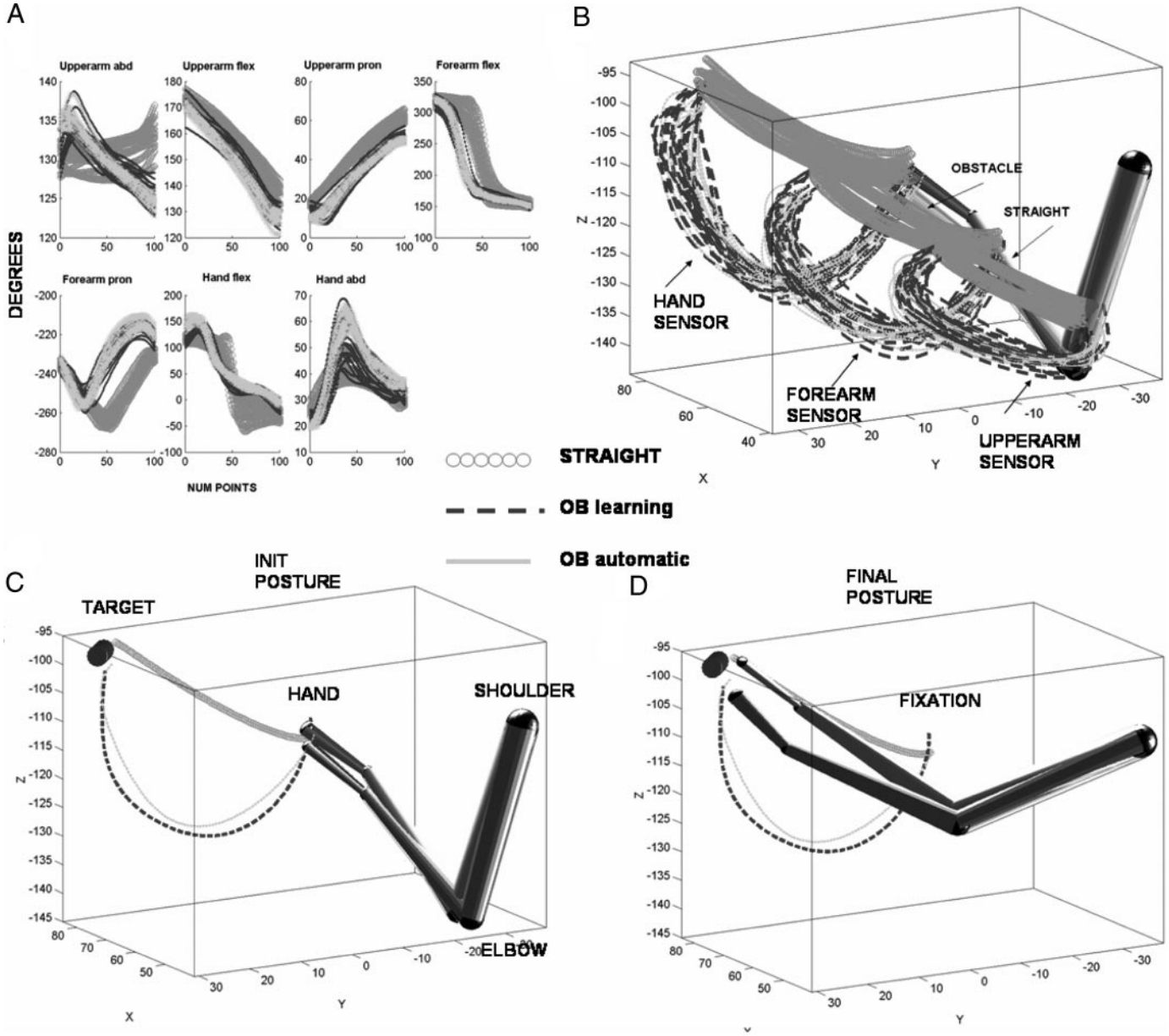

FIG. 5. *A*: paths (in degrees) of 7 joint angles of the arm recovered from the sensors placed at the hand, the forearm, and the upper arm. *B*: motion sensor path reconstruction aligned to the actual sensor paths for all 3 phases of movement. Spatial hand path consistency of OB-avoidance extended to the fore- and upper-arm levels. *C*: spontaneous repositioning of the arm at the beginning of the motion resulted in different initial postures between the straight and the OB reaches. *D*: final postures differed between straight and obstacle reaches.

tions, solely and inevitably as a result of the constraints imposed by the feedback delays in the system. If this was the case, the temporal point would have a constant value across the region of interest in the workspace regardless of the task condition or the spatial target location. Alternatively, in addition to the system's biological constraints there could be a strategic value for the time to reach the first peak velocity that would change as a function of the space location of the targets and of the goals imposed by the task condition.

To examine this question we analyzed two cases: *1*) for the same OB configuration and same starting hand location, does the temporal point shift as a function of the target location?; and *2*) for the same starting location of the hand and the same final target location, does the temporal point change as a function of the task condition? (i.e., for the contexts of no obstacle, one obstacle, two obstacles).

In the first case, we found that for both ipsi- (Fig. 8*A*) and contralateral (Fig. 8*B*) target locations, the same obstacle configuration (two OB) across 20 trials shifted the time to reach the first peak as a function of space location. Hand motions to location 11 reached the first peak at 250 ms on average before starting the deceleration phase of the movement. Hand motions to board location 2 reached the first velocity peak at 300 ms on average. The first OB that the hand passed by affected the temporal point with a significant effect for different target locations {one-way balanced ANOVA for ipsilateral targets on board locations 2 and 11; [$F = 72.75 > (F^*_{0.05,1,38} = 4.10, F^*_{0.01,1,38} = 7.35)$, $P = 0$, and $F = 19.65$,

TABLE 2. *Further analysis of postural paths*

	Insilateral Targets														
	Board Location 1					Board Location 6					Board Location 11				
	1–2	2–3	3–4	4–5	5–1	1–2	2–3	3–4	4–5	5–1	1–2	2–3	3–4	4–5	5–1
Time to First VP	1	0	0	1	0	1	0	0	0	0	1	0	0	0	0
(*P* value)	(0.08)	(0.57)	(0.53)	(0.08)	(0.29)	(0.03)	(0.64)	(0.37)	(0.61)	(0.33)	(0.0)	(0.79)	(0.37)	(0.26)	(0.57)
PL to First VP	1	1	0	1	0	1	0	0	0	0	0	0	0	0	0
(*P* value)	(0.03)	(0.05)	(0.14)	(0.05)	(0.14)	(0.01)	(0.18)	(0.62)	(0.38)	(0.93)	(0.33)	(0.32)	(0.20)	(0.38)	(0.25)
First VP value	1	1	0	1	0	1	1	0	0	0	1	0	0	0	0
(*P* value)	(0.02)	(0.02)	(0.41)	(0.03)	(0.39)	(0.0)	(0.0)	(0.41)	(0.32)	(0.38)	(0.0)	(0.76)	(0.29)	(0.30)	(0.58)
	Contralateral Targets														
	Board Location 5					Board Location 10					Board Location 15				
Time to First VP	0	0	0	1	0	1	0	0	1	0	1	0	0	0	0
(*P* value)	(0.6)	(0.68)	(0.78)	(0.04)	(0.15)	0.0	(0.67)	(0.31)	(0.03)	(0.79)	(0.0)	(0.76)	(0.2)	(0.27)	(0.26)
PL to First VP	1	0	0	1	0	1	0	1	1	0	1	0	0	0	0
(*P* value)	(0.0)	(0.9)	(0.96)	(0.01)	(0.1)	(0.0)	(0.13)	(0.04)	(0.02)	(0.16)	(0.0)	(0.74)	(0.11)	(0.28)	(0.57)
First VP value	0	0	0	1	0	1	0	1	0	0	0	0	0	0	0
(*P* value)	(0.44)	(0.43)	(0.82)	(0.02)	(0.24)	(0.02)	(0.29)	(0.0)	(0.55)	(0.79)	(0.38)	(0.22)	(0.16)	(0.38)	(0.26)

Columnwise comparison and *t*-statistics are as presented in Table 1. Parameters of interest are: the time to reach the first velocity peak in milliseconds, the distance traveled up to that time (path length PL to first velocity peak VP) in centimeters, and the value of the first velocity peak in centimeters/second. The time to first peak ranged from 200 to 320 ms for ipsilateral targets and from 220 to 420 ms for contralateral targets. Path length traveled up to the first peak ranged from 13 to 32 cm for ipsilateral targets and from 22 to 50 cm for contralateral targets. The first significant velocity peak value ranged from 75 to 150 cm/s for ipsilateral targets and from 105 to 160 cm/s for contralateral targets.

$P = 0$] for contralateral targets on board locations 5 and 15}. In the cases of board locations 2 and 5 the second OB that the hand passed by on the way to the final target was also taken into consideration for the subsequent temporal search.

In the second case, for the same starting location of the hand and the same final target location on the board, we found that the task condition significantly shifted the value of the temporal point both for ipsi- and contralateral targets. Figure 9 shows the hand paths to contralateral target on board location 5, the corresponding speed profiles, and the ANOVA results for all three conditions taken across 20 trials. As in the previous case, within a given task condition the time to reach the first velocity peak was consistent across all trials, but it shifted significantly from straight reaches to reaches around one obstacle, to reaches around two obstacles with a monotonically increasing trend [$F = 52.1 > (F^*_{0.05,2,57} = 3.16, F^*_{0.01,2,57} = 5.01), P = 0$]. This was also the case for the most affected ipsilateral target on board location 1 with a reversed monotonically decreasing trend (means were: no OB 226.5 ms, 1 OB 236.7 ms, 2 OB 248.7 ms; $F = 6.1$, $P = 0.005$).

Task switching

The experiment took place in the dark, yet the subjects saw both the positioning and the removal of the obstacle in full light. In switching from the straight to the curved reaches the goals and constraints imposed by the perceptual system dominated the choice of path strategy. A straight path to the target would have collided against the obstacle, but the system immediately solved this problem with a highly curved path. The perceptual goals were different from those of simple reaches and they determined the hand paths.

In switching from the automatic OB-avoidance reaches back to the straight reaches the perceptual goals were the same: reach for a spatial target. However, during the OB block the motor system had developed dynamics that did not comply with the straight reaches in demand. The arm system had to build the right inertial forces to enable very fast motions along many of the curved paths that did not overshoot the targets. In this case, the system in charge of the dynamics overrode the perceptual system, so residual curved paths with inadequate speed profiles for straight reaches were observed. Figure 10, *A* and *B* shows the hand positional paths for ipsilateral target on board location 1 and for contralateral target on board location 5. This kind of persistence resembles the notion of an "after-effect" observed in learning studies involving exposure to force fields (Shadmehr and Mussa-Ivaldi 1994).

Contralateral motions were more difficult because they required more stretching across the body to reach for the final targets. More variability was observed at the initial and final points of the motion. Table 1 (*columns 4* and *5*) displays significant differences in the spatiotemporal parameters of interest when comparing the first five to the last five trials of the deadaptation stage in the early days of experiment for the most affected targets (board locations 1 and 5). In particular, the first peak velocity value was statistically different for these targets during the early deadaptation.

These features extended to the joint angle domain. Figure 11*A* displays the joint angle paths also capturing the differences in endpoint paths despite the fact that the final spatial goal was the same. These residual paths were also observed in the forearms and the upper arms, which is depicted in Fig. 11*B* together with the differences in the initial and final postures.

Notice that in the previous transition from straight to OB-avoidance reaches, there were also differences in the initial posture from the very first trial. These different initial postures were in anticipation of a pending motion, one that the system had not yet executed, but for which the visual goals were more complex (obstacle-related in addition to target location). In the

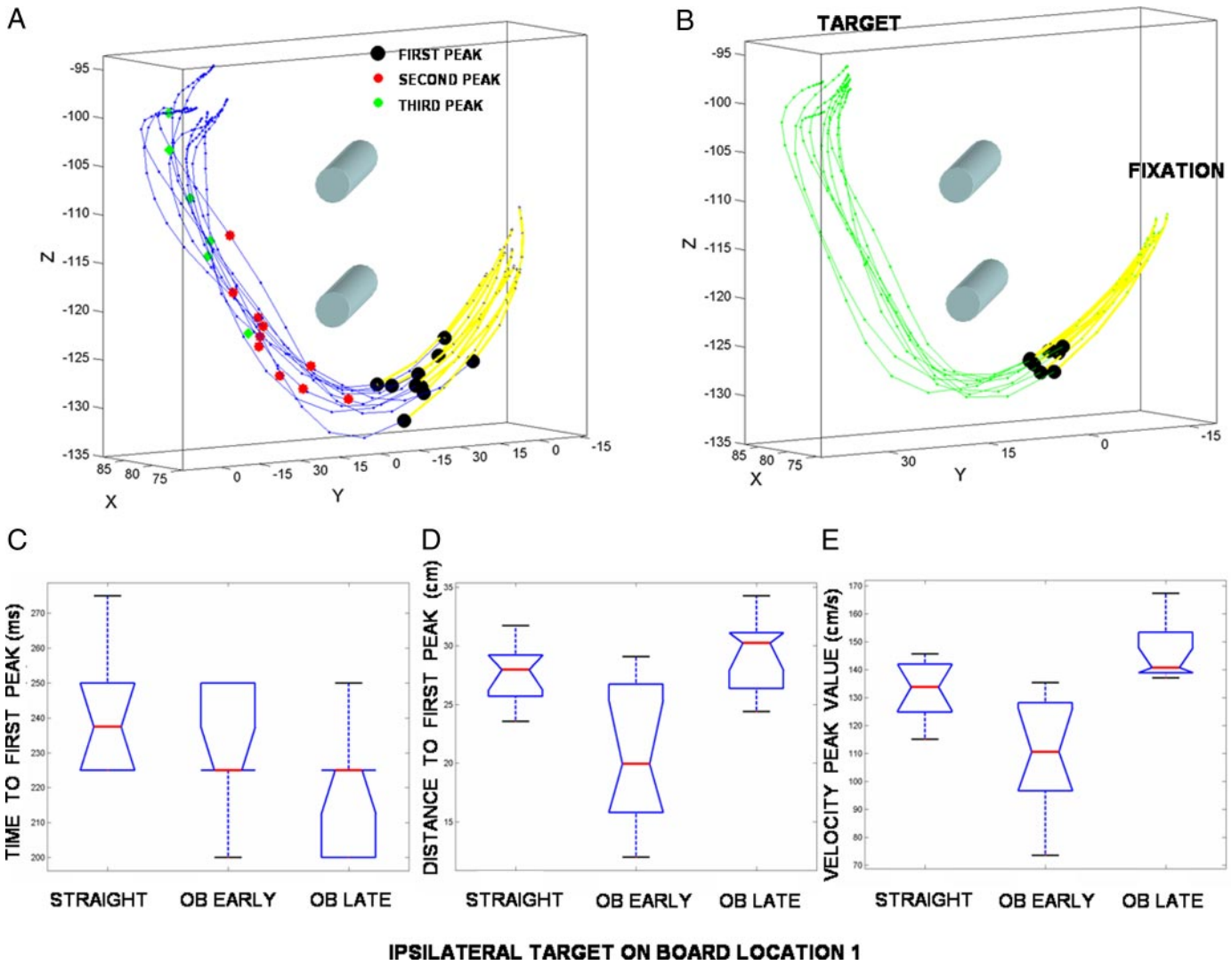

FIG. 6. First 10 trials vs. last 10 trials in the obstacle-avoidance block. *A*: black dots are at the end of the distance traveled up to the 1st velocity peak along the conserved paths. Partial distances are highlighted in yellow. These points were reached consistently at the same time (between 200 and 250 ms). Second peaks are red dots, 3rd peaks are green dots. *B*: systematically probing the distance traveled up to the 1st peak led to convergence toward a single spatial location for the point along the path where the 1st peak was reached (cluster of black dots). This was possible because of the consistency in the full spatial path and the constancy of the time for the 1st impulse. *C*: ANOVA results showed no learning effect on the time to reach the 1st peak velocity. ANOVA plots box and whisker for each condition. Box has lines at the lower quartile, median, and upper quartile values. Whiskers are lines extending from each end of the box to show the extent of the rest of the data. Outliers (a + sign) are data points with values beyond the ends of the whiskers. *D*: significant learning effect for the distance traveled up to the time to 1st peak. *E*: significant learning effect for the value of the peak velocity.

current case however, the visual goals were the same but the motor system was in a dynamics state that was not compliant with the straight reaches in demand. The differences in initial posture in this case were dominated by the motor end. Over time the system learned to perform this motor (dynamics) transformation in one step. This is depicted on Fig. 12, for the most affected contralateral target. After 15 days, task switching became automatic. OB-avoidance motions were significantly faster than those in the first day (one-tail critical *t*-test for 2 groups at the 0.01 alpha-level).

DISCUSSION

The data presented here clearly distinguish the learning from the automatic phases of motor skill acquisition, showing that initially—during the learning phase—space and time are separable. The spatial path of a complex motion was resolved before the system found the adequate temporal course to travel along that path. Temporal consistency emerged over time and led to the kind of space–time synchronization characteristic of "second-nature" movements. Once the system reached this level of automaticity it was no longer possible to decouple space and time.

This division suggests differential roles for the perceptual and the motor systems during the acquisition of a new motor skill. It poses the question of whether different but necessarily interrelated brain areas are involved in the learning and the automatic phases.

The spatial solution path for the new complex motion was resolved before movement execution. The best evidence for the precomputation of a spatial solution path lies in three facts.

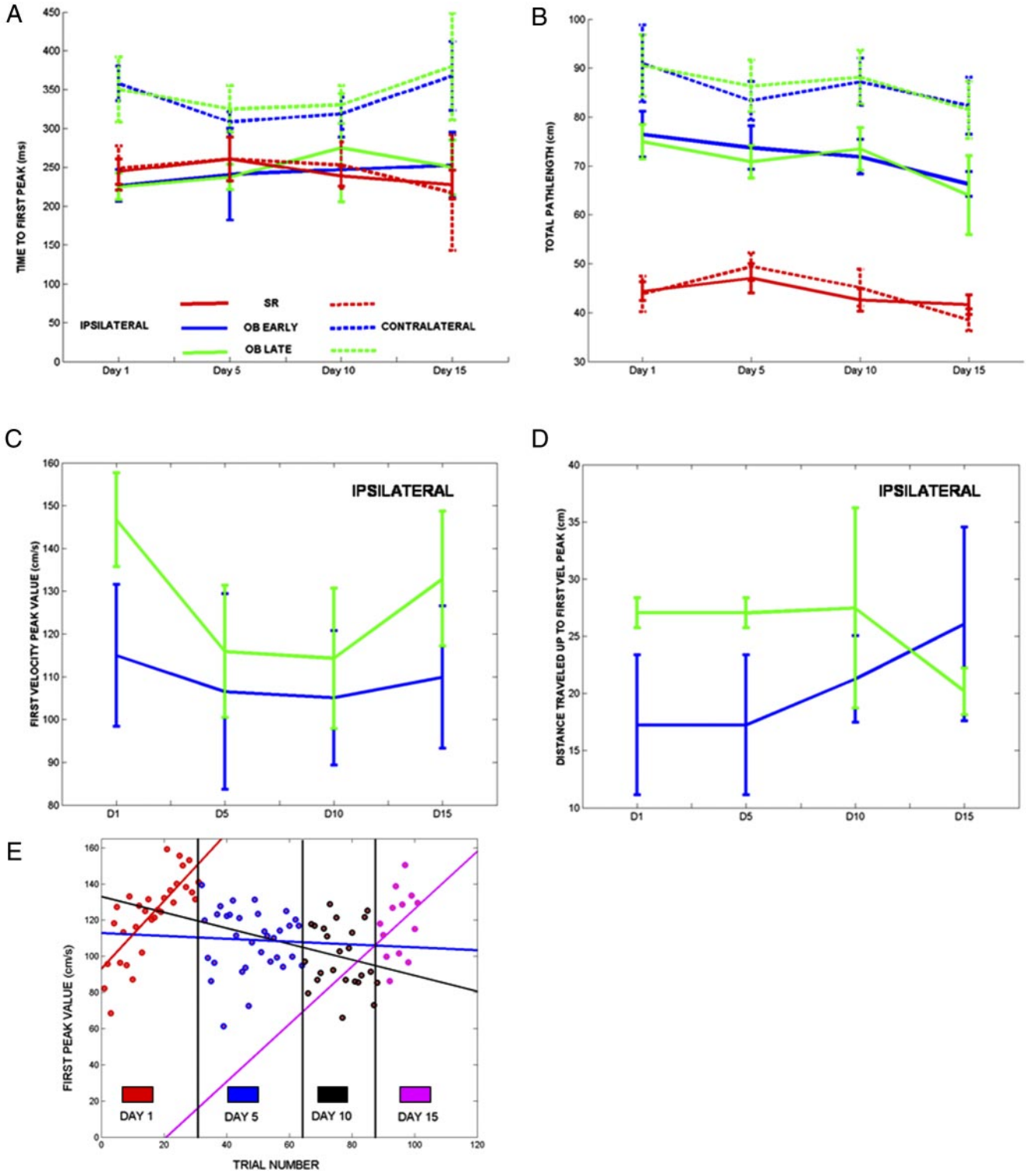

FIG. 7. *A*: time to reach the first significant velocity peak was robust to learning across time. Ipsi- and contralateral temporal points of interest were different and remained so over time. There were no differences in ipsi- and contralateral cases for the straight reaches. Error bars are symmetric of unit SD. *B*: path length remained fixed each day for both ipsi- and contralateral targets with a tendency to decrease across time. *C*: peak velocity value significantly differed between learning and automatic OB reaches in day 1 but tended to overlap days later. *D*: learning effect on the distance traveled up to the time to reach the peak velocity. Initially separable values tend to overlap after days of training as the value of the peak velocity monotonically increases and reaches a plateau. *E*: scatter of the 1st peak velocity values across the experimental trials of days 1, 5, 10, and 15 in the order in which they were performed and the least-square line fit for each day.

1) The task success in both animals from the first trial of the obstacle exposure in complete darkness.

2) The conservation of this path not only at the hand level but also at the forearm, the upper-arm, and at the postural level in six of the seven joint angles measured, while the temporal learning was evolving.

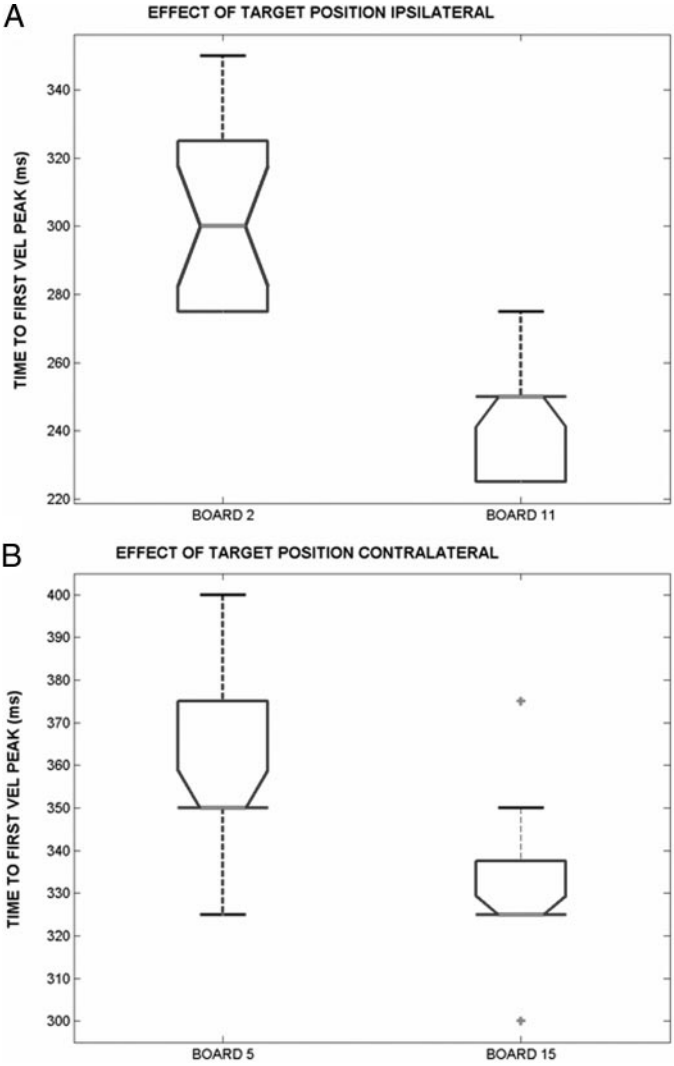

FIG. 8. Time to reach the 1st velocity peak depended on the target position in space. *A*: ANOVA plots showing a significant effect of target space locations on the temporal point (for the same obstacle configuration and same initial hand position) for ipsilateral targets. *B*: ANOVA significant effect in the case where targets are contralateral.

3) The spontaneous repositioning of the arm (change in initial posture) in anticipation of the obstacle-avoidance path.

This result implies that the perceptual system is involved not only in the identification of goals (target, obstacle, time to first peak) but also in the computation of the ideal spatial solution path for the task. The length of this ideal path plays a role in the estimation of movement duration for the computation of the optimal dynamics by the execution system. Spatial hand path constancy versus temporal path search hints that the former can be used as a reference while the latter is being learned.

These arm motions were unconstrained and occurred in three dimensions with ample room for other choices of hand path across different trials. Not only were the hand paths conserved but also the forearm and the upper-arm paths did remain invariant while the temporal course of the motion was dramatically changing. This spatial consistency extended to the joint angle paths recovered from the arm motion sensors. This is important because with more joint angles to control than dimensions in the perceptual goals, different postural solution paths across trials could have easily emerged as the system searched for the adequate temporal strategy. The joint-angle path robustness to drastic changes in temporal profiles suggests that the set of perceptual goals had an analogous set in the joint-angle space.

In particular, the postural adjustments observed before the obstacle-avoidance reaches set the stage for the new geometry-compliant dynamics. Before the movement started both animals determined already what portion of the space to use and translated that to the postural domain by rotating the arm to a posture more compliant with the OB-target configuration and the curvature of the upcoming path, which was executed 1 s later. Previous experimental work on pointing (Soechting et al. 1995) and orientation matching (Torres and Zipser 2004) showed that the initial position of the arm determines the final posture. Our present result on the postural paths extends these notions to a more complex task. In the context of task switching the spontaneous repositioning of the initial posture in anticipation of different dynamics is a new result that also agrees with the theoretical prediction that the joint-angle paths contain high-level cognitive information about the goals (Torres and Zipser 2004) and that, in addition to the final posture, the entire path depends on the initial posture (Torres and Zipser 2002).

A priori temporal information

The data revealed the existence of a temporal value that seemed important in shaping the evolution toward the final temporal course along the path. The perceptual system had a mapped representation of the time to reach the first velocity peak that smoothly varied across the target spatial locations and, within each spatial location, smoothly changed across tasks. This new result lends further support to our proposition that the motion's time is a dependent variable of the task space.

The representation of this particular temporal parameter was not subject to learning as was the full temporal course of the motion. While the value of the first velocity peak was changing (thus causing a change in the temporal duration under a fixed total path length), the time to reach this peak remained robust across days. This kind of movement feature is a good candidate for a motor primitive in trajectory formation. Whereas spatial features of the target object, such as location, orientation, shape, volume, and luminance, are identified by the visual system, it is an open question what system would identify this kind of temporal primitive for action. It is known, however, that the posterior parietal cortex (PPC), an early area involved in reference frame determination to locate spatial targets for action (Zipser and Andersen 1988), is also involved in the mental representation of the temporal aspects of simulated movements (Sirigu et al. 1996). It is possible that a space–time map for action exists in this area and is modifiable through experience as the tasks' demands change.

Just as the spatial goals determined the consistent spatial strategy, the time to first impulse clearly set perceptual constraints for trajectory generation. This is important because path generation between two points in space is an overcomplete problem. There are infinite numbers of ways to connect these points in space and time, yet having reliable spatiotemporal goals entirely determined the solution trajectory.

Another key aspect of these data were how early in the movement the peak velocity value was being updated as the

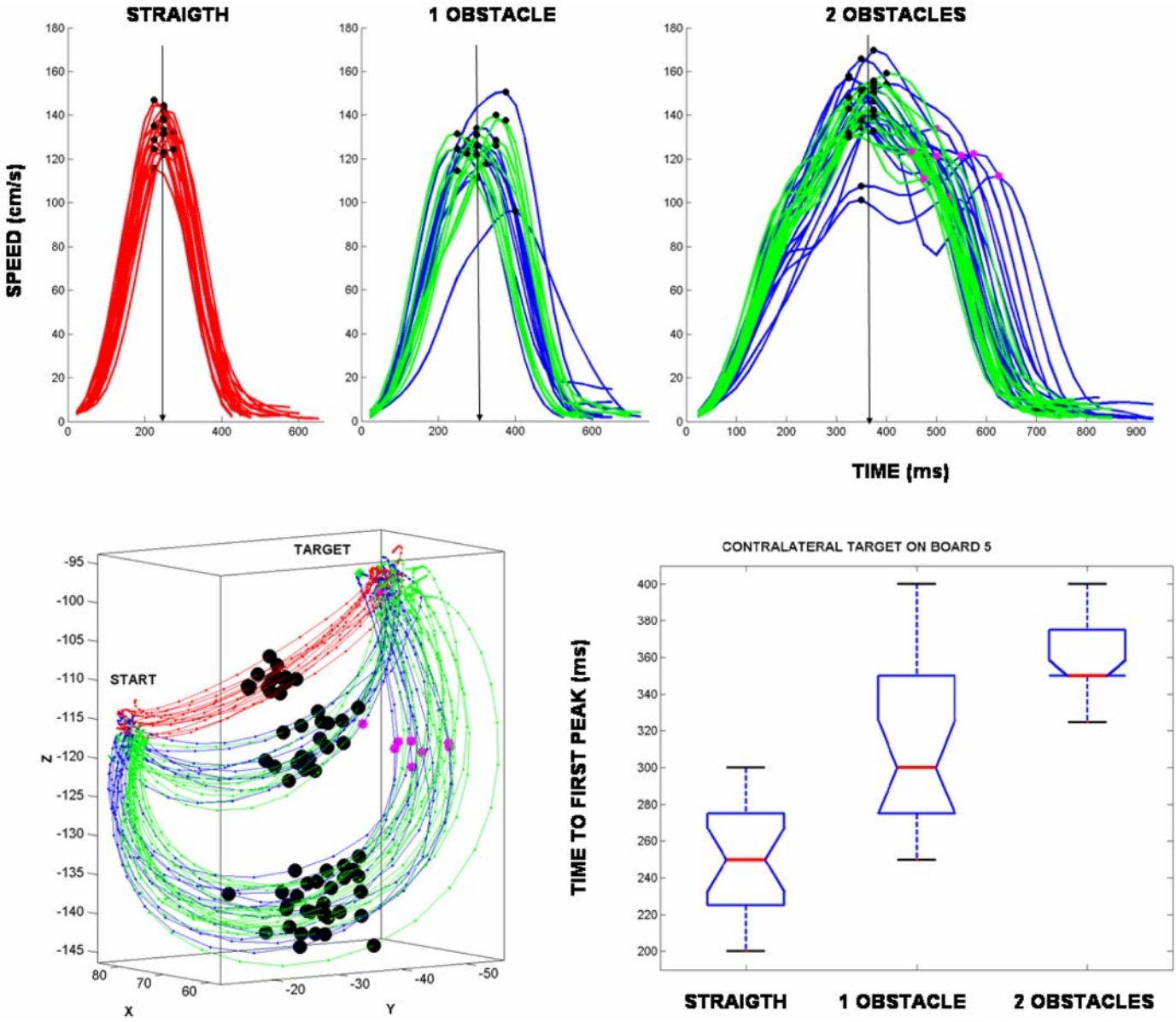

FIG. 9. Time to reach the 1st velocity peak depended on the obstacle configuration (task condition effect). Hand trajectories to contralateral target on board location 5 and corresponding speed profiles are shown for 3 conditions: no OB, 1 OB, and 2 OB. Movements started from the same board location (the fixation point). Red trajectories are straight reaches. In the 1- and 2-obstacle conditions, blue trajectories are OB-learning, green trajectories are OB-automatic. Black dots are the points along the path where the 1st peak was reached. Magenta stars for the 2-OB condition are the points along the trajectories where the 2nd velocity peak was reached. Effect is significant according to one-way ANOVA.

system was probing how far along the path the hand could travel before starting to slow down to stop at the target. For instance, Fig. 6, *A* and *B* shows the evolution of the distance traveled up to the first peak, where all the points at the end of this first impulse were reached between 200 and 250 ms. At 250 ms there was not enough time to receive sensory feedback from the motor component of the signal, yet at the execution of each trial the value of the velocity peak was being changed under cognitive control.

Speed is distance traveled in time. For a fixed time to first peak, this suggests that the kind of speed information under control came from a geometric distance-based estimation that could be obtained before the motion execution and bypass the time delays that sensory-motor feedback is subject to. This is in contrast to a temporal-based computation derived from the dynamics of the executed action. A good candidate for this type of fast and early, dynamics-invariant planning is the PPC because it seats between earlier perceptual and later motor areas. In particular we suggest the parietal reach region (PRR) as a region of interest for this kind of on-line learning mechanism. This processing would engage the perceptual (rather than the motor system) and rely on an abstract, geometric reference signal for the early portion of the movement. It was recently reported that rTMS causing disruption of the intraparietal sulcus in the PPC impairs correction during the first impulse of the motion (Glover et al. 2005). Lesions of this area cause severe misreaching behavior as well (Karnath and Perenin 2005).

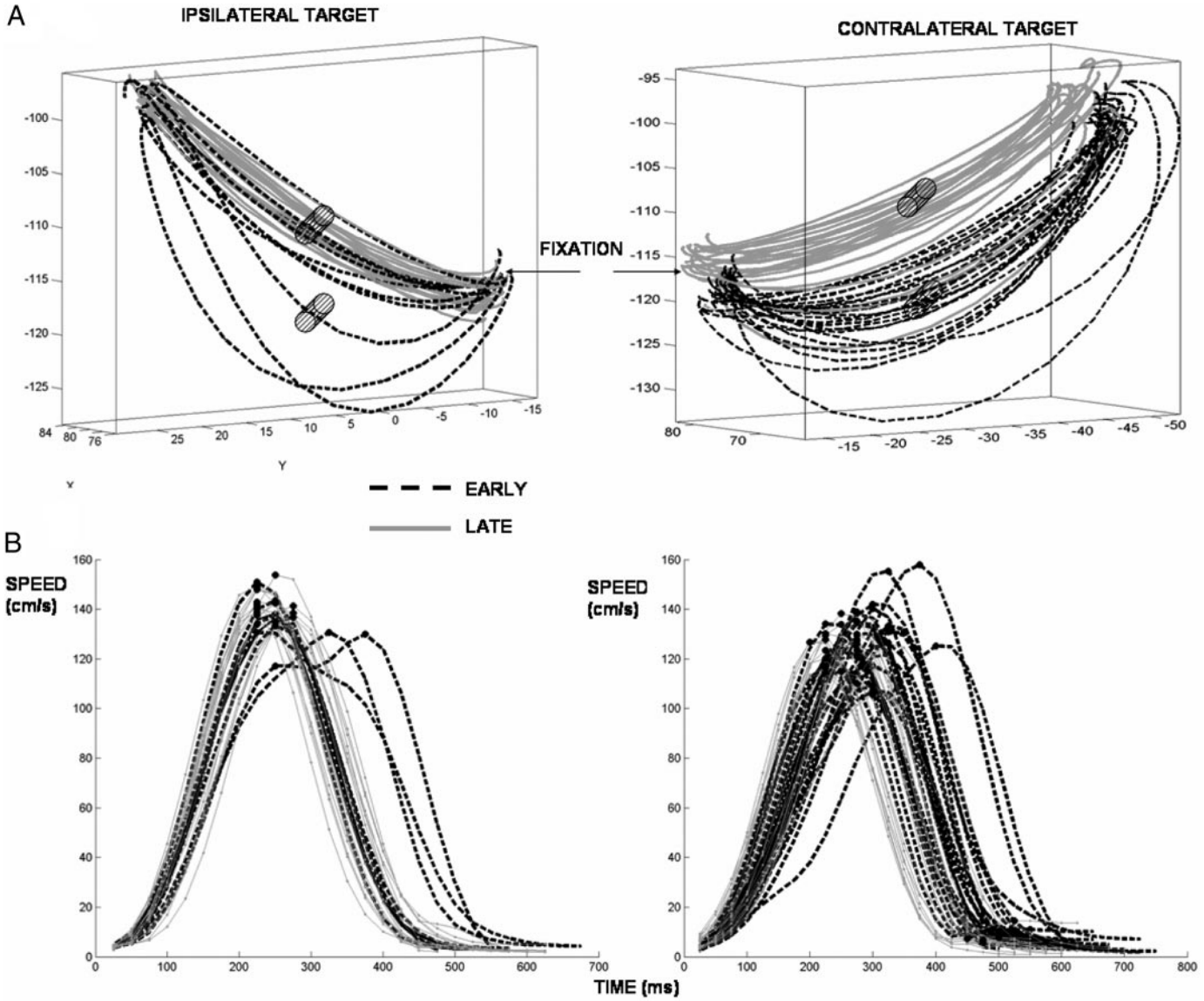

FIG. 10. *A*: OB-avoidance residual motions (dashed) in the spatial domain during early deadaptation. *B*: residual effects in the temporal strategy affected the peak velocity value, the time duration, and the point in time where the 1st peak is reached (dashed).

Theoretical implications of these results

The data described here suggest that a form of action simulation takes place before actual movement execution. There is an important difference between the types of planning that our data suggest and those that have dominated the computational field for many years (for recent reviews see Jordan and Wolpert 1999; Todorov 2004). Earlier optimal control models (Alexander 1997; Flash and Hogan 1985; Harris and Wolpert 1998; Todorov and Jordan 2002; Uno et al. 1989, 1995) solved the planning problem in a coupled manner, whereby a detailed spatiotemporal trajectory was generated before movement. In such models space and time are coupled. Regardless of whether the planning was based on extrinsic or intrinsic parameters, time in these models was predefined, so they could not account for temporal learning. None of these methods captures the flavor of our data: that paths are anticipated before the movement takes place, show an immediate spatial strategy, the paths are time invariant, and that the first impulse of the motion is under cognitive control. The type of precomputation that best characterizes our data is geometric—i.e., independent of the motion dynamics—yet provides a signal ready for the execution system.

During the learning period of motor skill acquisition this signal can be characterized using Hamilton–Jacobi's principle of least action from variational mechanics (Feynman 1965; Jose and Saletan 1998; Lanczos 1970). This principle considers mechanical systems whose Lagrangian function does not contain time explicitly and brings out the relationship between conservative systems and the non-Euclidean geometry of the underlying space. In particular the path in the learning stage can be thought of as the shortest straight line (a geodesic) between two definite endpoints in a Riemannian manifold.

We previously proposed that the brain simulates its actions in this space before execution (Torres and Zipser 2002). It is a space that links perceptual goals to an abstract representation of the biomechanical system that solves the dynamics of

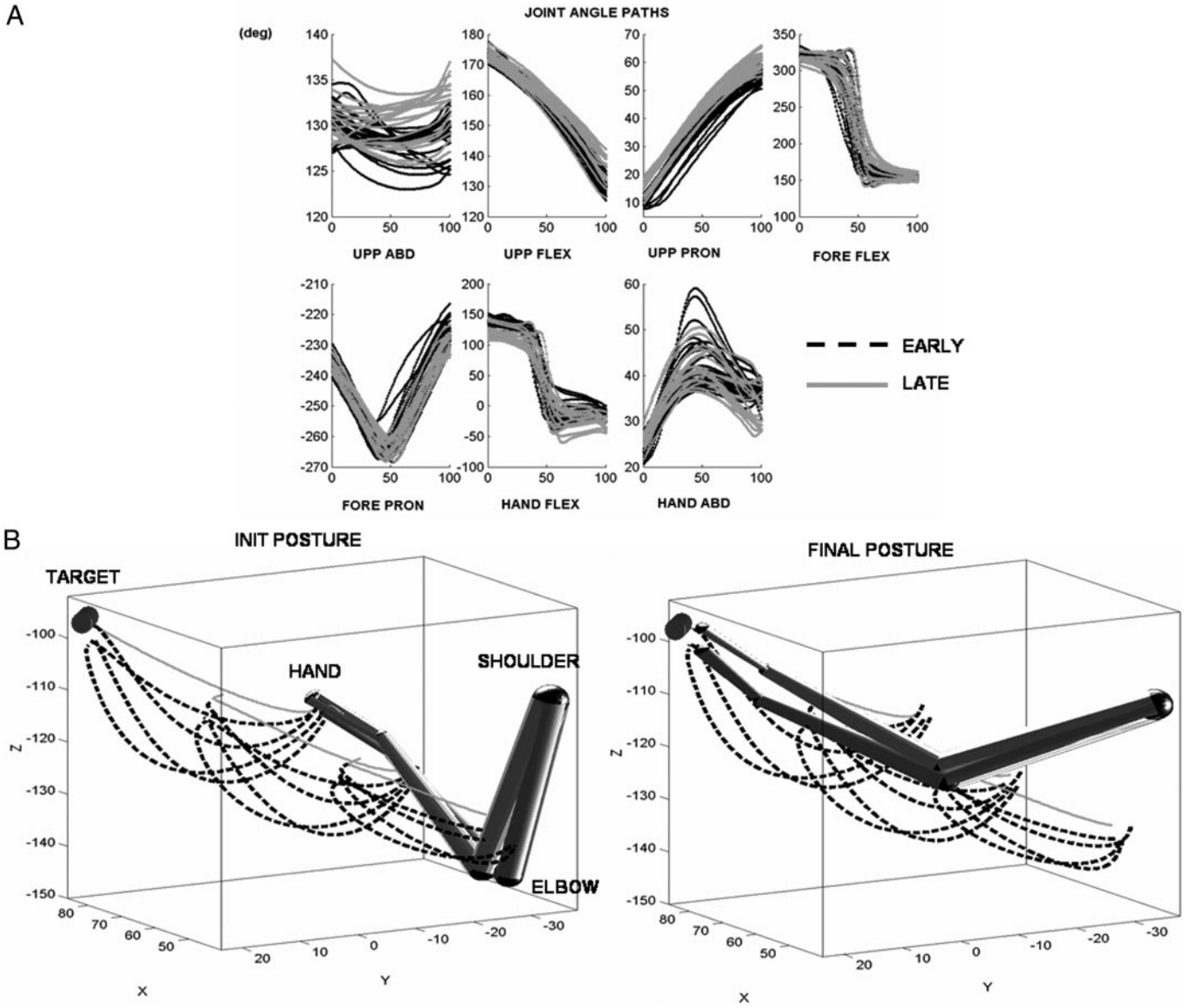

FIG. 11. *A*: deadaptation effects extended to the joint angle domain. *B*: average path for the last stage of the block is contrasted with the 1st 4 paths of the block. Residual paths at the hand extended to the fore- and the upper arms. Initial and final postures averaged over the 1st and the last 4 trials were different.

motion. Thus the simulated action contains perceptual information about the cognitive goals of a given task already translated to the language of the actual biomechanical system. What the principle of least action establishes is that the problem of finding the solution of a given dynamical problem is mathematically equivalent to the problem of finding the geodesics of the underlying space.

This simulated signal for action was recently modeled (Torres 2001) as a geodesic direction that coexists at the visual and the proprioceptive levels (see APPENDIX). According to this model there are two possible ways to generate the motion path: *1*) iterative path computation, which allows on-line error correction; and *2*) recursive spatial integration of the geodesic direction before motion execution, to provide the length of the geometrically optimal path for the dynamical system. The precomputed time-independent path is not a detailed description of the actual movement. It is neither the most optimal path of the dynamics, but it brings the system to a "good enough" configuration that solves the task. This path contains key spatial information that facilitates its dynamical implementation and temporal estimates linked to distances and geometric properties of the task. When coupled to the execution system this signal will lead to the efficient time course of the geometric movement.

Motions that are still being learned versus those that have reached automaticity can be thought of as simulated actions that are separable in space and time, as opposed to physical actions that can no longer be decoupled. The former are best described by a time-independent process. The motion path exists in space independent of time and can be well characterized as the solution to a time-independent partial differential equation. It answers a simpler question of "*how to get from point A to point B in space.*" Time at this stage depends on the task space and enters into the learning process.

In contrast, the solution path that solves a time-dependent integral describes the motion simultaneously in space and time.

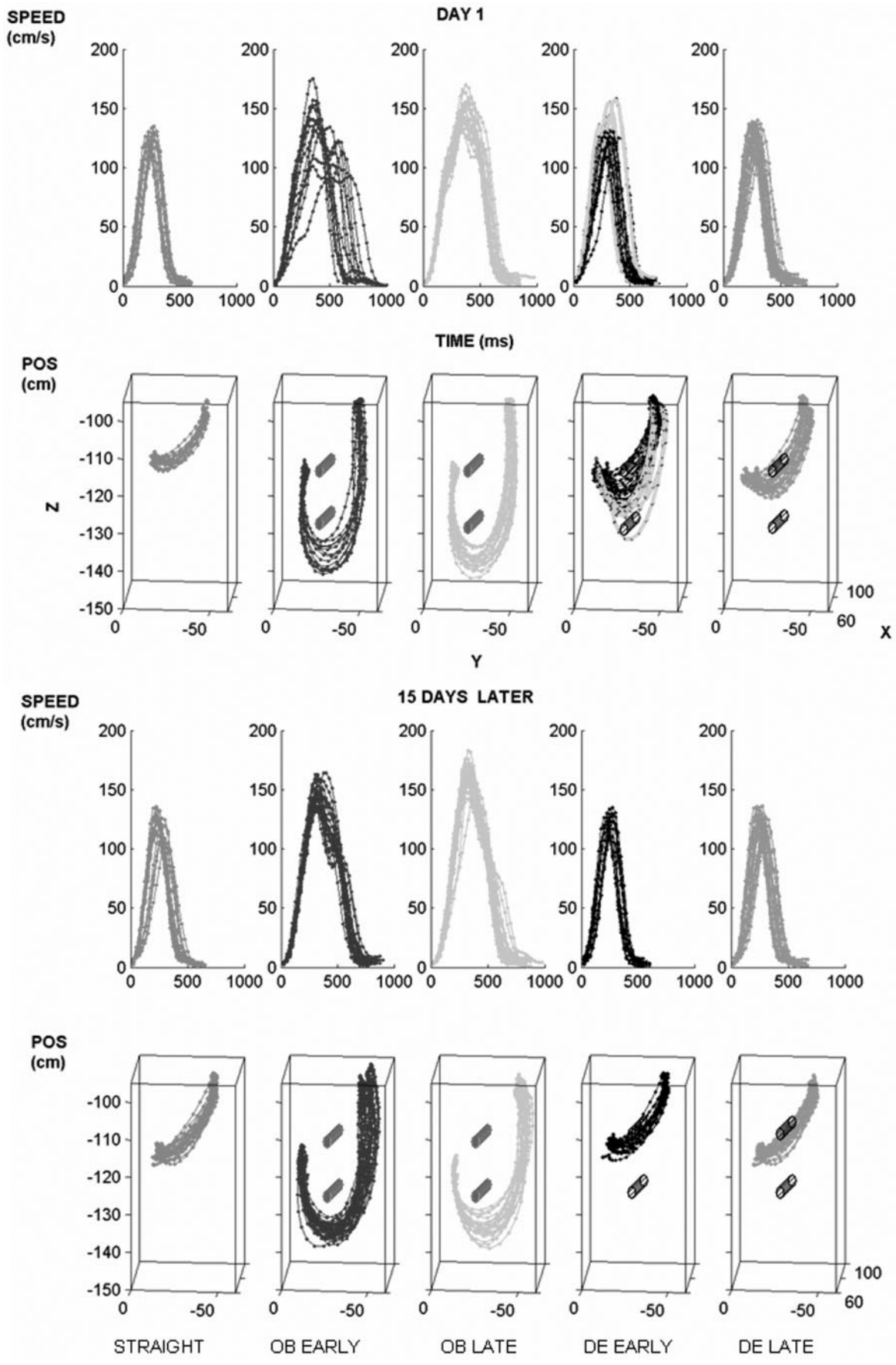

This characterization better suits the kinds of behaviors that are automatic. It answers a more complex question: "*how to get from point A now to point B exactly X ms later?*" Before this study it was never justified in the computational arena where the limits of integration for the dynamics were chosen from for the predefined time interval involving a given motion. It was simply always assumed that the system had a good estimate of what the duration of a given movement was before its execution.

In fact experimental work in motor control has reinforced this notion for many years. If one carefully reads the METHODS sections of many papers, one can see that subjects are instructed to perform motions within a predefined time window and receive some form of feedback on their success at it. These paradigms can afford such instructions because these simple motions were learned during infancy. There is no motor learning of the kind described here taking place during those experiments. A good estimate of movement duration is quite automatic.

Exquisite a priori temporal estimation of the entire motion might indeed exist for movements that have reached automaticity. However, we have empirically shown here that for a new task this notion emerged later with practice and repetition, and that early during the learning process, time was not a free variable. Its duration and course (speed profile) had to be learned.

From a computational perspective our results clearly establish a new kind of motion planning that is separable from the motion execution. The intermediate geometric planning stage proposed to exist in the PPC (Torres and Zipser 2002, 2004) acts as a translator between perceptions and actions. Its output provides an abstract representation of the motion that decouples space and time. This simulated action can be used as reference for its dynamics implementation. It was recently shown that the disruption of the parietal system impairs the learning of trajectory adjustment under new dynamics conditions (Della-Maggiore et al. 2004).

New experimental paradigm useful to study motor learning

In its current block-design form, the experimental paradigm's switching from one task to another resulted in a temporal visuomotor adaptation that over time permanently altered the relationship between the two tasks. As the obstacle-avoidance behavior reached a permanent automatic nature, task switching from straight to OB-avoidance reaches and back occurred in one step.

This new experimental paradigm will have implications for the neurophysiological aspects of this problem. Two distinct but necessarily interrelated cortical regions must be involved in geometric-based learning and the acquisition of automaticity, respectively. Neurophysiologists can use this paradigm in concurrent recordings of the PPC (which we target as the geometric transformer) and the M1 cortex (which we propose to be involved in the acquisition of motor coordination and temporal-based motor programs). Although both areas will be engaged through feedback loops, the PPC should lead initially while the motion is still geometric, i.e., separable in space and time, and its output must be used by the execution system. Yet later when the goal of space–time synchronization prevails and the system strives for a well-coordinated motion, M1 should lead and be highly and differentially engaged.

The subjects in our experiment had no visual feedback about the obstacle. It is an open question whether changing the task by lighting the peripheral obstacle while fixating straight ahead would change the trajectories' evolution. This is predicted because the underlying geometry of the perceptual space would change as well. An explicitly cued spatial via point could accelerate the temporal learning required to make the motion automatic. Simple modifications to the current paradigm will enable us to further investigate this and other important questions.

The present experimental results have implications for the understanding of the acquisition of a new motor skill in general because they formally distinguish learning from automaticity. The data show that temporal learning is separable from spatial learning in that it occurs later, it takes longer to master, and that over time it causes a permanent alteration of the visuomotor transformation relating an old well-known task to the new one. The performance of the new task also changes permanently, as it becomes "second nature," thus signaling the acquisition of a new motor program. This suggests that in a new task, the temporal aspects of the motion enter in the motor error signal for learning. It also suggests that temporal adaptation is crucial for the achievement of good motor coordination as defined by the tight synchronization of space and time. We have clearly shown that the temporal course for a new complex motion and its duration cannot be arbitrarily predefined when the system is faced with its geometry for the first time.

APPENDIX

The brain can perceive the external world through various sensory modalities but it has no direct access to it. In primates, the arm system and the hands serve as a mediator between the outside world and the brain's internal representation of the body. Our work proposes that when faced with a goal-oriented action (such as for survival or reproduction) the brain has the ability to simulate its internal representation of the body as constrained by the goals in the outside world before the actual action takes place. This is a mathematical model of that ability. Its details were previously described in a theory and instantiated in the context of reaching and reach-to-grasp motions (Torres 2001; Torres and Zipser 2002, 2004). The theory provides a general equation

$$d\boldsymbol{q} = G^{-1} \cdot \nabla \boldsymbol{r}^{task} \circ \boldsymbol{f}(q^{init}, x^{goals}) \cdot \Delta\tau \qquad (A1)$$

This equation transforms goals in the external world into their internal representation so that the system can simulate what the internal course of the action would be like in the outside world. Such an abstraction of the action exists independent of the dynamics of the actual motion in the physical world, so it remains invariant to dynamics-related changes. It relies on the perceptual system and serves as guidance to the motor system.

Path determination to achieve the set of goals in a given purposeful action comes from following a geometrically optimal direction (a geodesic direction) in posture and in hand space generated with *Eq.*

FIG. 12. Learning effect over time shown for raw data of the sensor at the hand of one subject. Trajectories were to one target on board location 5 (contralateral). Contrast between the 1st day and 15 days later of consecutive experiments. Automatic OB-avoidance motions became faster across blocks. On day 15 the transition from straight to early OB reaches did not show temporal learning. Transition from late OB-automatic to early DE-learning occurred in one step.

A1. The function **f** maps the initial posture $\mathbf{q}^{init}$ to the starting location of the hand and $\mathbf{x}^{goals}$ defines the goals of the task. Our optimization scheme defines **r**, the distance in **X**, as the objective function. The idea is to treat **r** as the line element of the spaces of interest.

The *line element* $\overline{\mathrm{ds}}$ denotes the infinitesimal distance between two neighboring points in space, expressed in terms of the coordinates and their differentials. In the Pythagorean case, $\overline{\mathrm{ds}^2} = \mathrm{d}x_1^2 + \mathrm{d}x_2^2 + \ldots$. This expression is a consequence of the Euclidean postulates and the coordinates x_1, x_2, ... However, if the coordinate lines of the reference frame system are no longer straight lines, but arbitrary curves, then the following general form is used instead

$$\overline{ds^2} = \sum_{i,j=1}^{n} g_{ij} dx_i dx_j$$

The g_{ij} term represents the coefficients of the special metric tensor, also known as the *First Fundamental Form* (Do Carmo 1992). They are the elements of a symmetric, positive, definite matrix, which in flat space is the identity matrix. In general, the matrix elements are constants only if rectangular, or more generally "rectilinear," coordinates (with oblique instead of rectangular axes) are used. In the case of curvilinear coordinates, values of g_{ij} change smoothly from point to point in space.

In our formulation, each task generates a different **r** distance in **X**, which is a function of the x^{goals}. For instance, the spatiotemporal goals in the obstacle-avoidance task relate to the obstacle location, the target, and the time to reach the first velocity peak. The composition of **r** with **f** builds a map $(\mathbf{r} \circ \mathbf{f}) : \mathbf{Q} \rightarrow \mathbf{X} \rightarrow R^{+}$, which is a function on **Q**. This construction is the *pullback* of **r** by **f**, denoted by $\mathbf{f}^{*}\mathbf{r} = (\mathbf{r} \circ \mathbf{f})$, which allows the control of the rate of change of **r** arising from changes in the set of joint angles representing a posture in **Q**.

In general

$$\boldsymbol{r}^{task} = \sqrt{\sum_{i=1}^{m} \sum_{j=1}^{m} g_{ij}^{\alpha} [f_i^{goals} - f_i(\boldsymbol{q})][f_j^{goals} - f_j(\boldsymbol{q})]}$$

where the g_{ij} term represents matrix coefficients for the metric in **X** and m is the number of goals spanning the dimension of **X**. In the Euclidean case, the g_{ij} terms constitute the Kronecker delta. For simplicity we start out with the Euclidean version and estimate the departure of the simulated paths from the real metric linked to the true data paths (Fig. *A*1). In this way, it is possible to compare different actions or how one action changes across different goals and con-

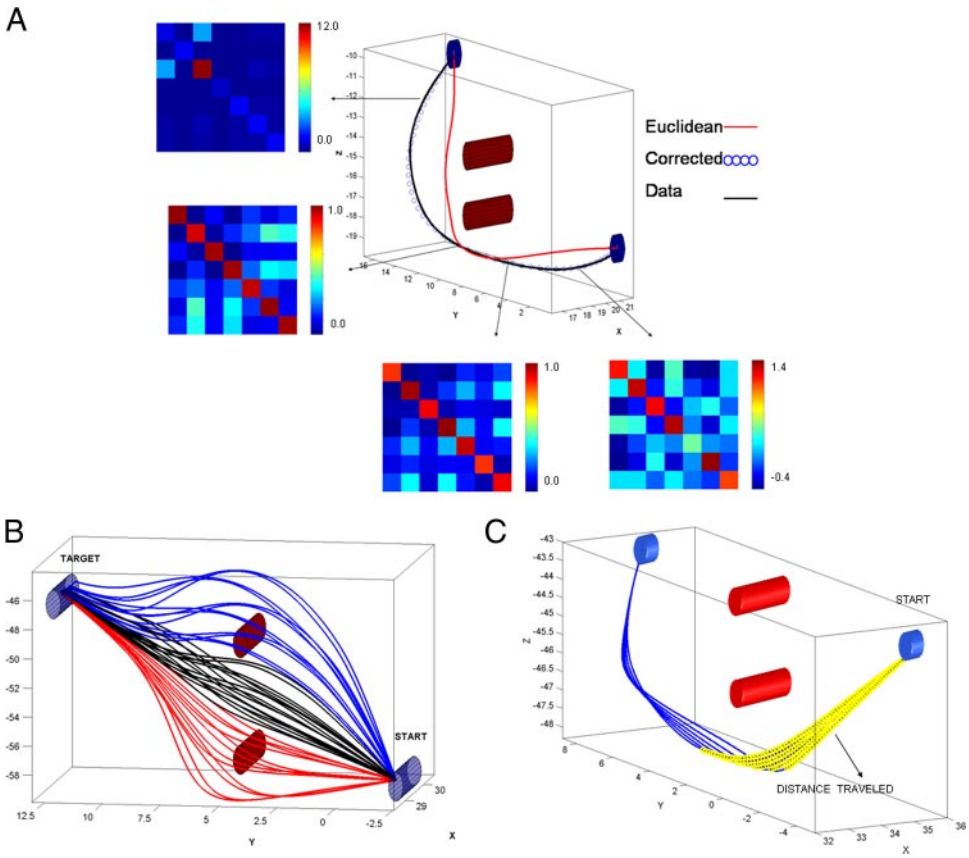

FIG. A1. *A*: average data and modeled hand paths (projected from posture space) to ipsilateral TARGET 1 on the board (for one monkey). The starting position is the fixation point. The safe area was set at around ⅓ of the spatial path. On average this corresponded to the point in time where the first significant velocity peak was reached (roughly *200–250 ms*) and *30 cm* were traveled. Notice the error between the modeled (red dot-line) and the veridical path (black line). This error can be estimated using a symmetric positive transformation matrix that brings the gradient modeled paths in joint angle space in register with the joint angle data paths (Torres and Zipser 2002). The coefficients of the transformation matrix can also be used as the new metric coefficients to transform the gradient vector originally computed under Euclidean metric. Equivalently one can think of a coordinate transformation that changes the $\boldsymbol{q}$-parametrization. Computing the gradient of $\boldsymbol{r}$ with new metric tensor $\overline{G}$ more suitable for the original $\boldsymbol{q}$-chart is equivalent to doing so after a coordinate transformation $\overline{\boldsymbol{q}}(\boldsymbol{q}) = G \cdot \boldsymbol{q}$ with metric G: i.e., $\overline{\nabla} r(\boldsymbol{q}) = \overline{G}^{-1} \cdot \nabla r(\boldsymbol{q}) = G^{-1} \cdot \nabla r(\overline{\boldsymbol{q}})$ (as in Torres and Zipser 2002). This transformation produces the corrected hand path (open circles). The 4 locations error matrix shown here along the path can be also used to numerically refine the true position-dependent metric coefficients. Along the path, the local transformation matrix is close to the identity, where the error between gradient-based path (generated under the Euclidean metric) and data path is minimal. *B*: the position of the safe region around the obstacle determines the path in space. Here we drive the paths through regions above, below and right through the obstacles using the general *Eq. A1* for the $\boldsymbol{r}$-distance in *Eq. A2*. *C*: for a location of the safety region it is possible to vary the desired distance traversed in the first impulse (D_1) and still keep the solution path within the same family.

straints. As explained in Torres and Zipser (2002), we operate on the gradient of $\mathbf{f}^*\mathbf{r}$, which we defined for simulations to gain insight into the true metric and its associated gradient from empirical data.

A geometrically optimal gradient—a geodesic direction—is obtained by pulling back into $\mathbf{Q}$ the geometry of $\mathbf{X}$ by its metric tensor and the *Jacobian*: $G_q^{\mu} = J^T G_x^{\alpha} J$, where G_x^{α} is an $m \times m$ matrix, J is $m \times n$, and G_q^{μ} is $n \times n$ (for simplicity we take $n = 7$ joint angles to represent postures). The G_q^{μ} is the new metric arising from the change of coordinates from $\mathbf{X}$ to $\mathbf{Q}$. It preserves the geometry of $\mathbf{X}$ through the G_x^{α} metric. In addition, it is also possible to modify the metric in $\mathbf{Q}$ to include other joint-angle constraints as in Torres and Zipser (2002). In tensorial language, the gradient in *Eq. A1* is a $\binom{0}{1}$-tensor, a covariant tensor of order one. The g_{ij} metric in E is a $\binom{0}{2}$-tensor conjugate to the g^{ij} metric in the space E^*, the dual of E, a $\binom{2}{0}$-tensor, i.e., $[g^{ij}]_{nn} = [g_{ij}]_{nn}^{-1}$. In *Eq. A1* applying $G^{-1} = [g_{ij}]_{nn}^{-1}$ to the covariant gradient raises the index to create a new contravariant $\binom{1}{0}$-tensor (Kay 1988), i.e., the differential $d\mathbf{q}$ that is tangent to the curve at each point describing the arm path. In what follows we denote $d\mathbf{q} = \tilde{\mathbf{q}}$.

The tensorial transformation in *Eq. A1* depends only on the relative orientations and scales of the coordinate axes at that point, not on the absolute values of the coordinates. It builds a local isometric linearization of the map $\mathbf{f} : \mathbf{Q} \subset E^n \rightarrow \mathbf{X} \subset E^m$, where $\mathbf{Q}$ and $\mathbf{X}$ are assumed to be open subsets of topological spaces with a norm, representing posture and cognitive spaces, respectively.

Preserving the notion of distance through the pullback operation makes the linear map $d\mathbf{f} : T_q\mathbf{Q} \rightarrow T_{f(q)}\mathbf{X}$ an isometry. Here the derivative map $d\mathbf{f}$ operates on the tangent spaces to the posture and the task manifolds, respectively. Let Y denote the vector field created by the transformation in *Eq. A1*, where each vector in the field is given by $Y_q = (\mathbf{q}, \tilde{\mathbf{q}})$ at each $\mathbf{q}$. Let Z denote a vector field in X, where each vector in the field is given by $Z_x = (\mathbf{x}, \tilde{\mathbf{x}})$ at each $\mathbf{x} = f(\mathbf{q})$. The derivative map $T_q f \cdot (Y) = (f_* Y)(\mathbf{x})$, is the *pushforward* of Y. It tells what the new vector field Z is in X under the transformation. Thus $\tilde{\mathbf{q}} \in T_q Q$ is pushed forward to get the geodesic direction $d\mathbf{x} = \tilde{\mathbf{x}} \in T_{f(q)}X$ at $\mathbf{x}$ (relative to the hand) by $d\mathbf{f}(\tilde{\mathbf{q}}) = \tilde{\mathbf{x}}$, where $\tilde{\mathbf{q}} = q^{\mathrm{T}} \oplus q^{\perp}$ in the sense of vector decomposition into the tangential and normal components, so that we can identify $\tilde{\mathbf{x}}$ with q^{T} in the subspace relevant to the task and distinguish it from the redundant dimensions.

The corresponding inverse map $d\mathbf{f}^{-1}$ starting at a given posture is locally injective, and the path thus obtained gives a continuous map onto its image $d\mathbf{f}^{-1}[T_{f(q)}X]$, i.e., an embedding (Do Carmo 1992). This local operation preserves in $\mathbf{Q}$ the notion of distance in $\mathbf{X}$ and makes $d\mathbf{f}^{-1}$ a local isometric embedding.

To guarantee that the direction $\tilde{\mathbf{q}} \in T_q\mathbf{Q}$ with $\mathbf{q} \in \mathbf{f}^{-1}(\mathbf{x})$ maps uniquely to the desired direction $\tilde{\mathbf{x}} \in T_{f(\mathbf{q})}X$, which the task demands, two conditions must be met.

1) $d\mathbf{f}(\tilde{\mathbf{q}}) = \tilde{\mathbf{x}}$, i.e., $\tilde{\mathbf{q}}$ maps linearly through the differential $d\mathbf{f}$ of the map $\mathbf{f}$ to the goal-related direction $\tilde{\mathbf{x}}$.

2) $\langle \tilde{\mathbf{q}}, \mathbf{q} + \tilde{\mathbf{q}} \rangle = 0 \; \forall \tilde{\mathbf{q}} \in Ker(d\mathbf{f}) = \{\tilde{\mathbf{q}} \mid d\mathbf{f}(\tilde{\mathbf{q}}) = 0\}$, i.e., $\tilde{\mathbf{q}} \perp \mathbf{q} + \tilde{\boldsymbol{q}}$ for all changes in postures that do not change the configuration of the hand (self-motion subspace). In this way one can restrict the solution to be the unique local geodesic direction $\tilde{\mathbf{q}} = \Delta\mathbf{q}$ for posture space with a corresponding direction $\tilde{\mathbf{x}} = \Delta\mathbf{x}$ for the hand space that iteratively builds the geodesic paths.

Equation A1 builds vector flows on the tangent spaces to the posture and the cognitive manifolds. The projection of such paths in three-dimensional space has curvature that should be informative of the underlying geometric changes that arise from changes in the task goals and constraints. *Equation A1* generates unit-speed paths (parameterized by arc-length) that minimize the $\mathbf{r}$-distance defined by the task. Notice that *Eq. A1* is recursive. It self-reevaluates the notion of distance and stops only when the value of $\mathbf{r}$ is 0, i.e., when all the goals are met. This generates paths autonomously. In addition, the iterative version allows coupling of the geometric signal with the dynamics. This is useful for on-line error correction (Torres and Zipser 2002) in the presence of sudden perturbations, adaptation, and so forth.

The $\Delta\tau$ refers to the step size for the unit-length gradient direction, and not to the time parameter for speed. During the first impulse of the motion $speed^{first} = d^{traversed}/time^{first}$ and by manipulating the value of the distance traveled to the first peak and/or the time to reach the first peak the system can change the magnitude of the first velocity peak. In this task for a given target location the time to the first peak remained constant, so changing the $d^{traversed}$ was equivalent to changing the magnitude of the speed. In terms of transmission delays in the motor system, this type of geometric manipulation can take place before the sensory motor feedback is available and engage the perceptual rather than the motor system.

When the reaching action involves obstacle avoidance the spatial path curves around the obstacle. To avoid overshooting the target or hitting the obstacle it makes sense to keep the $time^{first}$ constant while the system probes various speeds by changing the distance traversed in the first impulse until it settles on one that is optimal for the curvature of the path. In reaches along a straight path, however, the system can afford to peak midway to the target and rely on a symmetric strategy. In this sense moving at different speeds $speed^{first}$ for the first portion of the movement along the same path and conserving the strategy of $d^{traversed}$ to be half the total path length implies that the $time^{first}$ has to be systematically shifted [as subjects did in Torres and Zipser (2004)]. Both the temporal strategy for curved and that for straight reaches require early recruitment of the perceptual system to compute distances that are to be used within the movement initiation.

In this simplified version of obstacle avoidance we represent the main spatial goals, to avoid the obstacle (priority 1) and to reach the target (priority 2) while taking into consideration the partial $d^{traversed}$

$$r(\boldsymbol{q}^{init}, \boldsymbol{x}^{\boldsymbol{goals}})^{task} = \sqrt{\lambda_1 \sum_{i=1}^{3} [x_i^{safe} - f_i(\boldsymbol{q})]^2 + \lambda_2 \sum_{i=1}^{3} [x_i^{target} - f_i(\boldsymbol{q})]^2} \quad \text{(A2)}$$

The $\mathbf{x}^{\mathbf{goals}}$ include information about the safety region, the distance to be traveled during the initiation of the movement, and the target location. The minimizing paths depend on a safety region around the obstacle. Geometrically, this amounts to a "bend" in the shape of that part of the perceptual space that has to be pulled back into the posture space. The functions

$$\lambda_1 = \frac{1}{1 + e^{(d^{traversed} - D_1)}}$$

and

$$\lambda_2 = \frac{1}{1 + e^{-(d^{traversed} - D_2)}}$$

are weighting coefficients defining the two terms that drive the hand. It is an open question how the system disambiguates what the space region of interest should be. The data suggest that it is a function of the obstacle location, size, and shape in relation to how they constrain the distances from the body to the targets and obstacle locations. These distances form the space region where it is safe to move without colliding the limbs and/or the hand with the obstacles.

The driving terms depend on the distance traversed (which changes as the hand moves) and the fixed (desired) distances D_1 from the initial hand position to some place in the safety region, and (remaining) D_2 from that location to the target. Initially the term involving λ_1 dominates (is close to 1), pulling the hand toward the safety region and temporarily ignoring the target term (close to 0). As the hand approaches the safety area and avoids the obstacle, the second term involving λ_2 gains priority (approaches 1), and pulls the hand toward the target. The first term loses importance (λ_1 approaches 0). The heuristics of the task are encoded in these two functions so the hand autonomously moves to the target while avoiding the visual obstacle that is physically on the way to the target. Supplementary Fig. 1*B*

shows that hand paths are modulated by the safety region. This region can be visually specified above, below, or in between the obstacles, depending on other cognitive demands and physical constraints. Supplementary Fig. 1*C* shows how systematically changing the desired distance traveled in the first impulse (D_1) still keeps paths within the same family.

REFERENCES

Abend W, Bizzi E, and Morasso P. Human arm trajectory formation. *Brain* 105: 331–348, 1982.

Alexander RM. A minimum energy cost hypothesis for human arm trajectories. *Biol Cybern* 76: 97–105, 1997.

Atkeson CG and Hollerbach JM. Kinematics features of unrestrained vertical arm movements. *J Neurosci* 5: 2318–2330, 1985.

Della-Maggiore V, Malfait N, Ostry DJ, and Paus T. Stimulation of the posterior parietal cortex interferes with arm trajectory adjustments during learning of new dynamics. *J Neurosci* 24: 9971–9976, 2004.

Do Carmo M. *Riemannian Geometry.* New York: Springer-Verlag, 1992.

Feynman R, Leighton RB, and Sands M. *The Feynman Lectures on Physics*. Reading, MA: Addison–Wesley, 1965.

Flash T and Hogan N. The coordination of arm movements: an experimentally confirmed mathematical model. *J Neurosci* 5: 1688–1703, 1985.

Glover S, Miall C, and Rushworth F. Parietal rTMS disrupts the initiation but not the execution of on-line adjustments to a perturbation of object size. *J Cogn Neurosci* 17: 124–136, 2005.

Harris CM and Wolpert DM. Signal-dependent noise determines motor planning. *Nature* 394: 780–784, 1998.

Hatsopoulos NG, Paninski L, and Donoghue JP. Sequential movement representations based on correlated neuronal activity. *Exp Brain Res* 149: 478–486, 2003.

Jordan MI and Wolpert DM. *Computational Motor Control.* Cambridge, MA: MIT Press, 1999.

Jose JV and Saletan EJ. *Classical Mechanics: A Contemporary Approach.* Cambridge, UK: Cambridge Univ. Press, 1998.

Karnath H-O and Perenin M. Cortical control of visually guided reaching: evidence from patients with optic ataxia. *Cereb Cortex* 15: 1561–1569, 2005.

Kay D. *Theories and Problems of Tensor Calculus.* New York: McGraw-Hill, 1988.

Konczak J and Dichgans J. The development of hand trajectory formation and joint kinematics during reaching in infancy. In: *Three-Dimensional Kinematics of Eye, Head, and Limb Movements*, edited by Fetter M, Haslwanter T, Misslisch H, and Tweed D. Sydney, Australia: Harwood Academic, 1997.

Lanczos C. *The Variational Principles of Mechanics.* New York: Dover, 1970.

McNitt-Gray J. *Neuromuscular Control and Performance of Gymnastics Landing.* Oxford, UK: Blackwell Science, 2000.

Morasso P and Mussa-Ivaldi FA. Trajectory formation and handwriting: a computational model. *Biol Cybern* 45: 131–142, 1982.

Nishikawa KC, Murray ST, and Flanders M. Do arm postures vary with the speed of reaching? *J Neurophysiol* 81: 2582–2586, 1999.

Rencher AC. *Methods of Multivariate Analysis.* New York: Wiley, 1995.

Shadmehr R and Mussa-Ivaldi FA. Adaptive representation of dynamics during learning of a motor task. *J Neurosci* 14: 3208–3224, 1994.

Sirigu A, Duhamel J, Cohen L, Pillon B, Dubois B, and Agid Y. The mental representation of hand movement after parietal cortex damage. *Science* 273: 1564–1568, 1996.

Soechting J, Buneo C, and Flanders M. Moving effortless in three dimensions: does Donders' law apply to arm movement? *J Neurosci* 15: 6271–6280, 1995.

Todorov E. Optimality principles in sensorimotor control. *Nat Neurosci* 7: 907–915, 2004.

Todorov E and Jordan M. Optimal feedback control as a theory of motor coordination. *Nat Neurosci* 5: 1226, 2002.

Torres EB. Theoretical framework for the study of sensori-motor integration. In: *Cognitive Science.* La Jolla, CA: University of California San Diego, 2001, p. 115.

Torres EB and Zipser D. Reaching to grasp with a multi-jointed arm. I. A computational model. *J Neurophysiol* 88: 1–13, 2002.

Torres EB and Zipser D. Simultaneous control of hand displacements and rotations in orientation-matching experiments. *J Appl Physiol* 96: 1978–1987, 2004.

Uno Y, Fukumura N, Suzuki R, and Kawato M. A computational model for recognizing objects and planning handshapes in grasping movements. *Neural Netw* 8: 839–851, 1995.

Uno Y, Kawato M, and Suzuki R. Formation and control of optimal trajectory in human multijoint arm movement. Minimum torque-change model. *Biol Cybern* 61: 89–101, 1989.

Viviani P and Flash T. Minimum jerk, two-thirds power law, and isochrony: converging approaches to movement planning. *J Exp Psychol Hum Percept Perform* 21: 2–53, 1995.

Viviani P and Schneider RA. A developmental study of the relationship between geometry and kinematics of drawing movements. *J Exp Psychol Hum Percept Perform* 17: 198–218, 1991.

Wada Y and Kawato M. A via-point time optimization algorithm for complex sequential trajectory formation. *Neural Netw* 17: 353–364, 2004.

Zipser D and Andersen R. A back-propagation programmed network that simulates response properties of a subset of posterior parietal neurons. *Nature* 331: 679–684, 1988.